

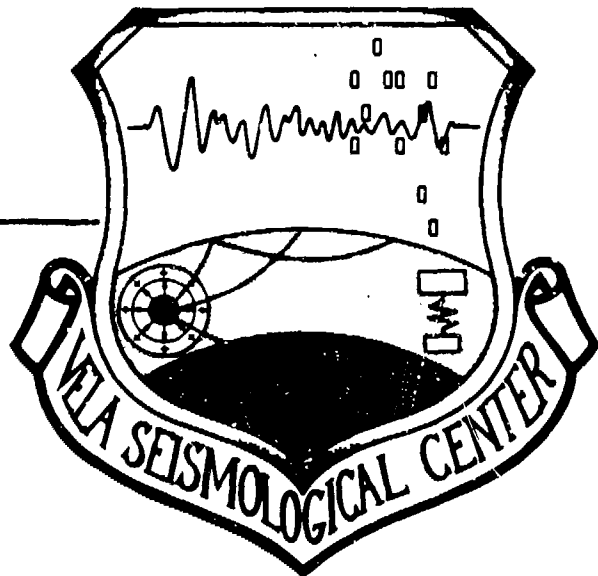
(12)

LEVEL II

AD A 099 446

VSC-TR-81-2

SEISMIC DETECTORS:
THE STATE OF THE ART



Jon Berger
Robert L. Sax (ENSCO, INC.)

SYSTEMS, SCIENCE AND SOFTWARE
P.O. Box 1620
LaJolla, California 92038

May 8, 1981

DTIC
ELECTED
MAY 28 1981
S D
B

APPROVED FOR PUBLIC RELEASE,
DISTRIBUTION UNLIMITED

DTIC FILE COPY

Monitored By:
VELA Seismological Center
312 Montgomery Street
Alexandria, VA 22314

81526030

AFTAC Project Authorization No: VT/0712/B/PMP
Effective Date of Contract: November 17, 1978
Contract Expiration Date: January 31, 1981
Amount of Contract: \$1,262,007
Contract No: F08606-79-C-0008
Principal Investigator and Phone No:
Dr. Thomas C. Bache, (714) 453-0060
Project Scientist and Phone No:
Major G. Wayne Ulrich, (202) 325-7561

THIS RESEARCH WAS SUPPORTED BY THE AIR FORCE TECHNICAL APPLICATIONS CENTER AND WAS MONITORED BY AFTAC/VSC, PATRICK AIR FORCE BASE, FLORIDA, 32925, UNDER CONTRACT NO. F08606-79-C-0008.

THE VIEWS AND CONCLUSIONS CONTAINED IN THIS DOCUMENT ARE THOSE OF THE AUTHORS AND SHOULD NOT BE INTERPRETED AS NECESSARILY REPRESENTING THE OFFICIAL POLICIES, EITHER EXPRESSED OR IMPLIED, OF THE ADVANCED RESEARCH PROJECTS AGENCY, THE AIR FORCE TECHNICAL APPLICATIONS CENTER, OR THE U.S. GOVERNMENT.

UNCLASSIFIED

SECURITY CLASSIFICATION OF THIS PAGE (When Data Entered)

18

VSC

19 TR-81-2

REPORT DOCUMENTATION PAGE			READ INSTRUCTIONS BEFORE COMPLETING FORM
1. REPORT NUMBER	2. GOVT ACCESSION NO.	3. RECIPIENT'S CATALOG NUMBER	
AD-A099446			
4. TITLE (and Subtitle) SEISMIC DETECTORS: THE STATE-OF-THE-ART.		5. TYPE OF REPORT & PERIOD COVERED Technical Report.	
6. AUTHOR(s) Jon Berger Robert L. Sax (Enesco, Inc.)		7. PERFORMING ORG. REPORT NUMBER SSS-R-80-4588	
8. PERFORMING ORGANIZATION NAME AND ADDRESS Systems, Science and Software P. O. Box 1620 La Jolla, California 92038		9. PROGRAM ELEMENT, PROJECT, TASK AREA & WORK UNIT NUMBERS VT/712/B/PMP	
10. CONTROLLING OFFICE NAME AND ADDRESS Vela Seismological Center 312 Montgomery Street Alexandria, Virginia 22314		11. REPORT DATE 8 May 1981	
12. NUMBER OF PAGES 94		13. SECURITY CLASS. (of this report) Unclassified	
14. MONITORING AGENCY NAME & ADDRESS (if different from Controlling Office)		15. DECLASSIFICATION/DOWNGRADING SCHEDULE	
16. DISTRIBUTION STATEMENT (for this Report) Approved for Public Release, Distribution Unlimited.			
17. DISTRIBUTION STATEMENT (of the abstract entered in Block 20, if different from Report)			
18. SUPPLEMENTARY NOTES			
19. KEY WORDS (Continue on reverse side if necessary and identify by block number) Seismic Detection			
20. ABSTRACT (Continue on reverse side if necessary and identify by block number) The following detectors were reviewed: 1. IBM; 2. Z; 3. Deflection; 4. Analytic Envelope; 5. Allen; 6. Stewart; 7. Walsh; 8. MARS. All these detectors are based on a comparison between some signal variance over a time period equal in deviation to the expected event and the normal or long time variance. Detectors using the phase have been suggested but not yet satisfactorily implemented. Uniform comparative testing of the detectors has not yet been done and is recommended. Additional research to improve detector			

388507

UNCLASSIFIED

SECURITY CLASSIFICATION OF THIS PAGE (When Data Entered)

ABSTRACT Continued

performance is needed to: 1. develop phase sensitive detectors; 2. determine the improvements possible with matched filters; 3. further develop hybrid algorithms that combine high detection probability/high false alarm rate algorithms with low false alarm rate post processors; 4. develop algorithms designed specifically for three-component, broad-band data; and 5. investigate the use of dedicated micro-processors to run the detection algorithms on a one processor per channel (or seismic station) basis.

Accession For	
NTIS GRA&I	<input checked="" type="checkbox"/>
DTIC TAB	<input type="checkbox"/>
Unannounced	<input type="checkbox"/>
Justification	
By _____	
Distribution/	
Availability Codes	
Dist	Avail. and/or Special
A	

TABLE OF CONTENTS

<u>Section</u>			<u>Page</u>
I.	INTRODUCTION		1
	1.1 DETECTION THEORY		1
	1.2 THE FRIEBERGER DETECTOR.		7
	1.3 TESTING DETECTORS.		11
II.	IMPORTANT SEISMIC EVENT DETECTORS		16
	2.1 IBM DETECTOR, VANDERKULK, <u>et al.</u> (1965)		16
	2.2 "Z" DETECTOR, SWINDELL AND SNELL (1977)		27
	2.3 DEFLECTION DETECTOR, SHENSA (1977)		36
	2.3.1 The Average Power Detector.		36
	2.3.2 The Maximum Deflector Detector.		38
	2.3.3 The Average Deflection Detector		38
	2.4 ANALYTIC ENVELOPE DETECTOR, FARNBACH (1975); UNGER (1978)		44
	2.5 ALLEN DETECTOR, ALLEN (1978)		57
	2.6 THE STEWART DETECTOR, STEWART (1977)		63
	2.7 WALSH DETECTOR, GOFORTH, T. AND E. HERRIN (1980) . .		71
	2.8 MARS DETECTOR, MASSO, <u>et al.</u> (1979).		77
III.	CONCLUSIONS AND RECOMMENDATIONS		84
IV.	ACKNOWLEDGMENTS		87
V.	ABSTRACTS OF PRINCIPAL PAPERS		88
VI.	REFERENCES.		95
	APPENDIX A: BIBLIOGRAPHY OF SEISMIC EVENT DETECTORS		97

LIST OF FIGURES

1.1	Probability density function of the H_0 and H_1 hypotheses.	2
1.2	The receiver operating characteristics (ROC).	4
1.3	Implementation of the Frieberger detector.	7
1.4	Threshold levels of STA/LTA of variance estimators for different false alarm probabilities.	9
1.5	Probability of detection: completely known signal (after Helstrom, 1968, p.106).	15
1.6	Receiver operating characteristics: completely known signal (after Helstrom, 1978, p. 107)	15
2.1	The IBM detector	17
2.2	Loss in performance of the noise-prewhitening filter for the IBM detector (after Vanderkulk, <u>et al.</u> , 1965).	19
2.3	Loss in performance caused by rectifying rather than squaring the prefilter output (after Vanderkulk, <u>et al.</u> , 1965).	22
2.4	Performance loss of an exponential integrating filter (after Vanderkulk, <u>et al.</u> , 1965).	25
2.5	Coda suppressor for the "Z" detector (after Swindell and Snell, 1977).	30
2.6	"Z" detector flow diagram (after Swindell and Snell, 1977)	32
2.7	"Z" detector LTA controller (after Swindell and Snell, 1977).	33
2.8	Block diagram of three deflection detectors showing how the scales statistic X, Y or Z is derived from the power spectrum $P_f(k)$ (after Shensa, 1977).	37
2.9	The complex analytic signal. A modulated carrier $f(t)$, its quadrature function $F_{H_1}(t)$, and the associated complex analytic signal are all shown as functions of the real variable time (after Bracewell, 1965).	45
2.10	Envelope representation of the complex analytic signal (after Bracewell, 1965).	47
2.11	The instantaneous phasor for the complex analytic signal (after Unger, 1978).	48

2.12	Envelope and phase probability distribution curves (after Unger, 1978).	50
2.13	Analytic signal detection and timing (after Unger, 1978).	52
2.14	Stepback procedure in analytic signal timing (after Unger 1978).	53
2.15	(a) Block diagram of the Allen detector and (b) the response functions of the two filter elements.	59
2.16	Schematic earthquake with data stored during events. (a) Seismic event with onset and end points. (b) Dots represent zero-crossing times and previous peak amplitudes. Amplitude bars indicate background noise preceding onset, and arrow gives first difference at onset. (c) Data stored for use by analysis routines after event terminates (after Allen, 1978).	60
2.17	Processing steps to compute the modified seismic signal MDX_k from the incoming signal X_k . The modified signal is used extensively in the detection logic of the on-line system (after Stewart, 1977).	64
2.18	Effect of the filtering operation (summarized in Figure 2.17) on a 1 Hz and 3 Hz sinusoidal signal. The upper signal is the unfiltered analog output of a function generator, fed simultaneously to one channel of the on-line system and to a chart recorder. The lower signal is the filtered function MDX_k , computed in real-time by the on-line system and routed through a digital-to-analog converter to the chart recorder. Digitizing rate is 50 samples/second. Peak amplitude of the 3 Hz filtered signal is approximately twice that of the 1 Hz signal (after Stewart, 1977).	65
2.19	The first eight Walsh functions.	72
2.20	Walsh detector flow diagram (after Goforth and Herrin, 1980). . . .	74
2.21	Typical t_g -f plane representation of a time series segment (0 to 36 sec.) when the signal-to-noise ratio is low. Only the largest envelope maxima (X) and second largest maxima (O) are shown. Other, numerous, smaller envelope maxima are normally scattered throughout the t_g -f plane, but for this illustration they have been omitted. Each filter "output line" normally displays about ten such peaks.	80
2.22	MARS detector flow diagram.	82

I. INTRODUCTION

1.1 DETECTION THEORY

The problem of the detection of a seismic signal, sometimes present, sometimes absent, in the presence of noise may be conveniently discussed using the theory of statistical detection. (See Helstrom, 1968, as a good general reference.) Based on a set of measurements, we are trying to choose between two hypotheses:

H_0 that the measurements consist only of noise

H_1 that the measurements consist of signal plus noise.

For discrete data, we can conveniently use matrix notation and represent the set of measurements as a vector \underline{x} with components x_i that are the individual samples of the seismometer's output (the detector's input).

The number of components, N , in this vector is the number of samples of the input that we consider (process) at one time. We can measure something about the characteristics or statistics of \underline{x} over a given time interval, and a signal may be detected if, over this interval, these input statistics are significantly different from what we would expect from noise alone. Now, obviously, we will maximize this statistical difference if we match this time interval to the finite duration of the expected seismic signal. This fundamental time duration, T_D , is typically on the order of a second, and a quantity calculated over this interval is often referred to as the "short term average" (STA) of the input signal. Thus the number of components in the vector \underline{x} will be

$$n = \frac{T_D}{\Delta t}$$

where Δt is the sampling interval.

The detector must decide between the hypothesis H_0 and H_1 . The correct strategy to use depends upon the cost or the risk of making the wrong decision. In seismic applications (as opposed to game theory for example) the cost or risk of making the wrong decision is impossible (or at least difficult) to quantify. Instead, what is commonly done is to use the Neyman-Pearson strategy which maximizes the probability of detection with a specified probability of being wrong - a false alarm. Conceptually, we can think of the process of hypothesis testing by using the probability density functions $p_0(\underline{x})$ and $p_1(\underline{x})$ of H_0 and H_1 .

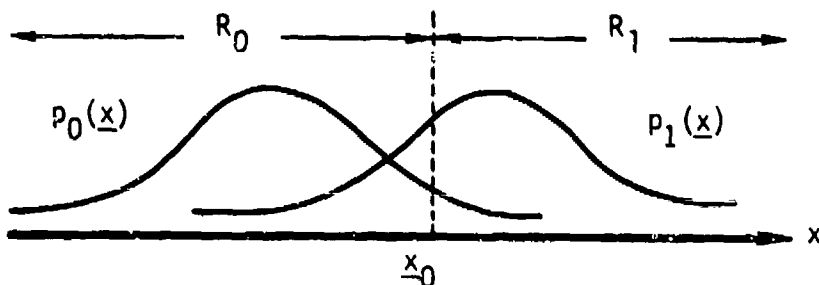


Figure 1.1. Probability density function of the H_0 and H_1 hypotheses.

The chance of error, Q_0 , caused by choosing H_1 when H_0 is true, that is "detecting" a signal when one is not there, is called a false alarm probability. It is given by

$$Q_0 = \int_{x_0}^{\infty} p_0(x) dx \quad (1.1)$$

Observe that:

1. The probability of false alarm, Q_0 , and the false alarm rate, FAR (number of false alarms per unit time), are related by a time interval T_D

$$\text{FAR} = \frac{Q_0}{T_D}$$

where T_D is the time interval (non overlapping) over which the "statistic" is calculated.

2. Increasing T_D decreases FAR for a fixed Q_0 but also decreases the time resolution of the detector.
3. Increasing T_D also provides for more frequency resolution for those detectors working in the frequency domain.
4. In the case where there is a signal present, increasing T_D will possibly decrease the signal-to-noise ratio (SNR) by including more noise after the signal has died away.

The error, Q_1 , of choosing H_0 when H_1 is true, that is, not detecting a signal when one is present, is given by

$$Q_1 = \int_{-\infty}^{x_0} p_1(x) dx \quad (1.2)$$

and the detection probability Q_D is

$$Q_D = 1 - Q_1. \quad (1.3)$$

The Neyman-Pearson strategy of decision theory leads us to search for the minimum Q_1 for a specified Q_0 . Ideally, for each detector we would like to be able to construct a diagram like Figure 1.2 which in detection theory is called the "receiver operating characteristic" (ROC).

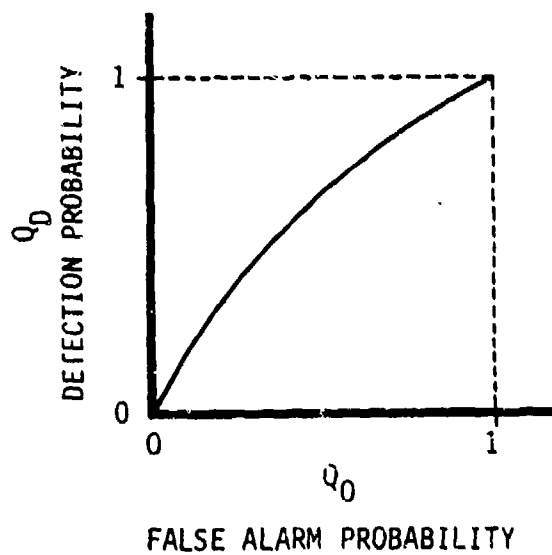


Figure 1.2. The receiver operating characteristic (ROC).

The slope of the ROC curve is

$$\frac{dQ_0}{dQ_0} = \Delta \equiv \frac{p_1(x)}{p_0(x)} \quad (1.4)$$

which is called the "likelihood ratio". This is easy to see as

$$Q_0 = 1 - Q_1 = \int_{-\infty}^{\infty} p_1(x) dx - \int_{-\infty}^{x_0} p_1(x) dx = \int_{x_0}^{\infty} p_1(x) dx \\ = \int_{x_0}^{\infty} \Delta(x) p_0(x) dx \quad (1.5)$$

$$Q_0 = \int_{x_0}^{\infty} p_0(x) dx \quad (1.6)$$

Thus

$$\frac{dQ_D}{dx} = \underline{\Lambda}(\underline{x}) p_0(\underline{x}) \quad \text{and} \quad \frac{dQ_0}{dx} = p_0(\underline{x})$$

so

$$\frac{dQ_D}{dQ_0} = \underline{\Lambda}(\underline{x}) \quad (1.7)$$

For example, in the case of a Gaussian signal in Gaussian noise,

$$p_0(\underline{x}) = \frac{1}{(2\pi)^{n/2} \sqrt{\det R_0}} \exp\left(-\frac{1}{2} \underline{x}^t R_0^{-1} \underline{x}\right) \quad (1.8)$$

$$p_1(\underline{x}) = \frac{1}{(2\pi)^{n/2} \sqrt{\det R_1}} \exp\left(-\frac{1}{2} \underline{x}^t R_1^{-1} \underline{x}\right) \quad (1.9)$$

where R_0 and R_1 are the covariance matrices of noise plus noise and \underline{x}^t is the transpose of \underline{x} . We see that the likelihood function

$$\underline{\Lambda}(\underline{x}) = k \exp\left(\frac{1}{2} \underline{x}^t (R_0^{-1} - R_1^{-1}) \underline{x}\right) \quad (1.10)$$

is a monotonic function of the quadratic form

$$\underline{x}^t \underline{A} \underline{x} \quad (1.11)$$

where

$$\underline{A} = R_0^{-1} - R_1^{-1} \quad (1.12)$$

As Helstrom (1968, p. 94) shows, the choice between hypotheses H_0 and H_1 can equally be based on any monotonic function of the likelihood function $\underline{\Lambda}(\underline{x})$. The quantity that summarizes and replaces that

data \underline{x} themselves is termed the detection "statistic". Clearly, then, we could equally well use the quadratic form

$$\underline{x}^t \underline{A} \underline{x}$$

as our detection statistic.

We may generate this statistic by the action of a linear filter \underline{H} on the signal \underline{x} followed by a device that forms the product

$$(\underline{H} \underline{x})^t \cdot (\underline{H} \underline{x})$$

since this is

$$\underline{x}^t \underline{H}^t \underline{H} \underline{x} = \underline{x}^t \underline{A} \underline{x} \quad (1.13)$$

It may be shown that if \underline{A} is a positive definite symmetric matrix,

$$\underline{H} = \underline{D} \underline{Q}^t \quad (1.14)$$

where \underline{D} is the diagonal matrix of the square roots of the eigenvalues of \underline{A} while \underline{Q} is the matrix of normalized eigenvalues of \underline{A} .

1.2 THE FRIEBERGER DETECTOR

In an elegant work by Frieberger (1963) it is shown that the quadratic form given by Eq. (1.11) can be approximated by a constant times the integral

$$\int_0^{\infty} F_x(\omega) \cdot \frac{F_s(\omega)}{F_N(\omega)[F_s(\omega) + F_N(\omega)]} d\omega \quad (1.15)$$

in the case where the signal and noise both have a Gaussian probability density function. In this equation, F_x , F_N and F_s are the power spectral densities of the input, the noise alone, and the signal alone, respectively. This detector can thus be implemented as illustrated in Figure 1.3.

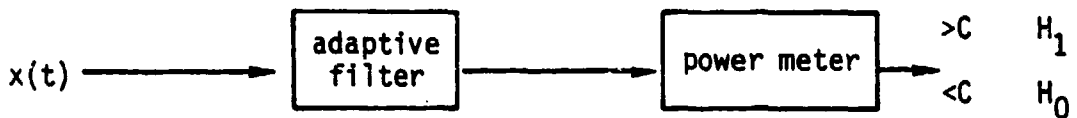


Figure 1.3. Implementation of the Frieberger detector.

where the modulus of the frequency response of the adaptive filter is given by:

$$\sqrt{\frac{F_s(\omega)}{F_N(\omega)[F_s(\omega) + F_N(\omega)]}} \quad (1.16)$$

and the power meter is a quadratic integrator. Because of the squaring operation, the filter phase response is irrelevant. Note that for a large SNR (i.e., $F_s(\omega) \gg F_N(\omega)$), this response is approximately $\sqrt{1/F_N(\omega)}$. It is not the Weiner filter which is $\sqrt{F_s(\omega)/(F_s(\omega) + F_N(\omega))}$, whose task is not to detect but rather to recover the signal.

What has become to be referred to as the "conventional power detector" simply performs the function of the quadratic integrator without Frieberger's pre-filter.

Over a short time interval (STA), say $n\Delta t$, an estimate is made of the variance. For the i^{th} epoch, this is simply

$$P_i = \underline{x}_i^T \underline{x}_i = \frac{1}{n} \sum_{j=1}^n x_j^2 .$$

To take the place of the adaptive prefilter, the long term average (LTA), say $m \Delta t$ duration, is calculated in the absence of a seismic event to provide an accurate estimate of the noise variance σ^2 . The ratio of these quantities, namely

$$\frac{P_i}{\sigma^2} ,$$

is then compared to a constant. For Gaussian random input data, this number is the ratio of two chi-squared random variables with $2n$ and $2m n$ degrees of freedom. Thus, the ratio follows the F distribution (Bendat and Piersol, 1971, p. 107). The expected value of the ratio is unity, and its variance is a function of m and n . For noise that is uncorrelated with the seismic signal, the conventional power detector estimates the statistic

$$\frac{S+N}{N} ,$$

where S and N are the signal and noise variances.

If the STA and LTA are both estimates of the variance of a normally distributed quantity, then the ratio STA/LTA is t - distributed with v_s, v_L degrees of freedom where

$$v_s = T_{STA}/ \Delta t \quad \text{The number of samples in the STA}$$

and

$$v_L = T_{LTA}/ \Delta t \quad \text{The number of samples in the LTA}$$

Figure 1.4 shows the dependence of threshold level C of STA/LTA on v_L for $v_s = 20$ and three different false alarm probabilities, that is

$$\text{Prob} [STA/LTA \leq C] = P_0 .$$

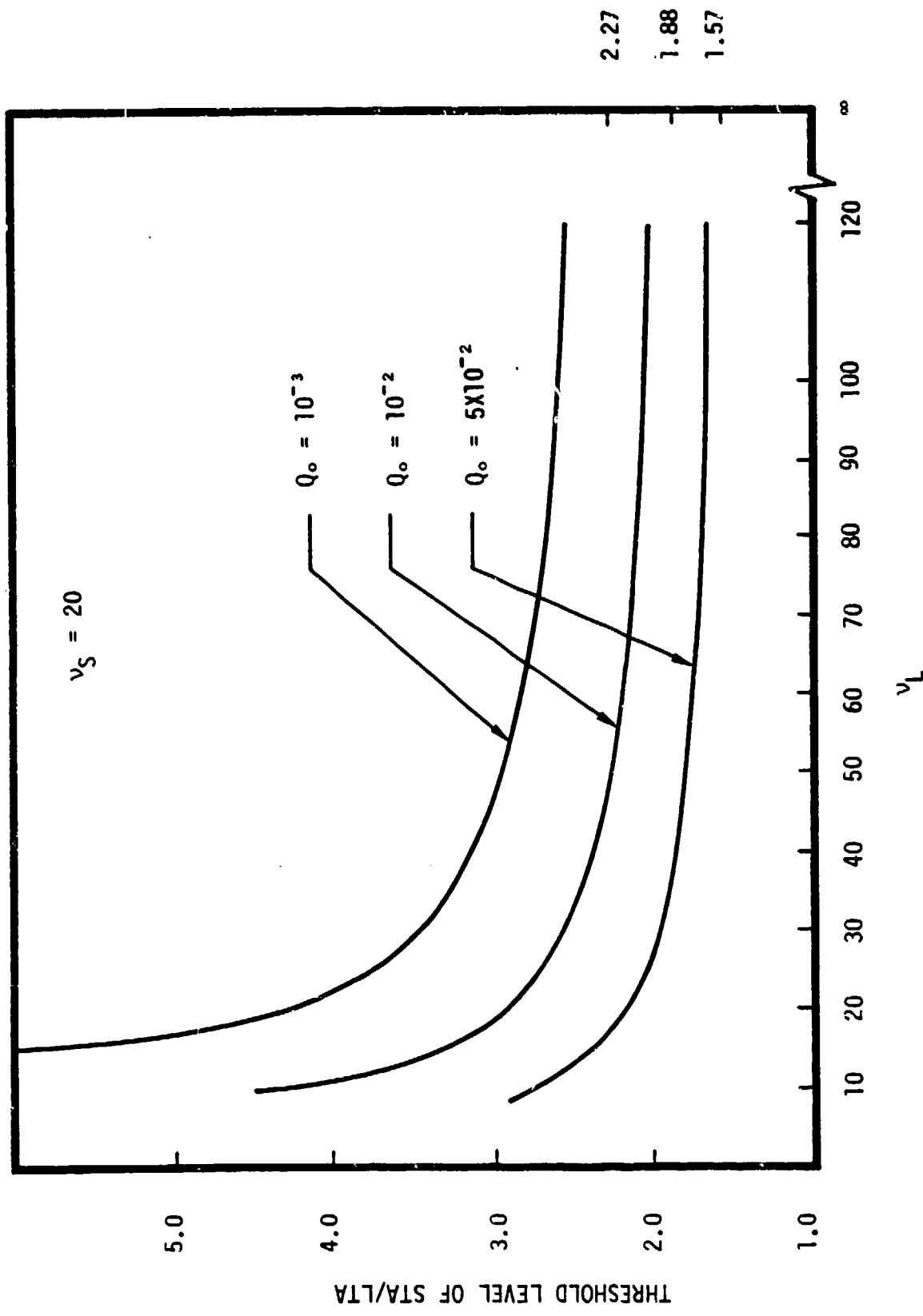


Figure 1.4 Threshold levels of STA/LTA of variance estimators for different false alarm probabilities.

Two interesting features can immediately be seen.

1. The is little to be gained in lengthening the LTA beyond the "knee" of these curves. For example, suppose the STA is 1 second for 20 sps data. Thus $v_L = 20$. With an LTA of only 6 seconds, $v_L = 120$ and the ratio STA/LTA will be less than 2.03 99 percent of the time and less than 2.53 99.9 percent of the time. Extending the LTA to an infinite period (perfect estimate) only reduces the thresholds to 1.88 and 2.27 respectively -- only a 0.33db or 0.47db improvement.
2. The change in the threshold levels as a function of false alarm probability is the other interesting feature. For $v_S = 20$ and $v_L = \infty$, Table 1.1 gives the FAR assuming a STA of 1.8 seconds.

Table 1.1

Q_0	5×10^{-2}	10^{-2}	10^{-3}	10^{-4}
FAR/hr	100	20	2	.2
Threshold in db	1.96	2.74	3.56	6.5C

Thus, with this STA period, setting the threshold at about 3 will achieve a FAR of about one per hour.

The basic ideas presented here are all well known and form the basis of almost all seismic detectors. The individual detectors discussed in later chapters differ in detail and implementation as each uses different methods in attempting to optimize the probability of detection for a fixed false alarm probability. They also reflect differences in assumed noise models and input data sets. Obviously, a

detector for low SNR teleseismic pulses will be different from a high SNR local event detector meant to be implemented in the microprocessor of a field recorder.

1.3 TESTING DETECTORS

For each detector, we would like to produce the Receiver Operating Characteristic (ROC) curves (Figure 1.2). These may be readily generated once the detector has been implemented. We simply generate a synthetic data set containing noise plus signals at known times and with specified SNR. Enough such data must be used to gather a meaningful statistical sample of the detector's performance.

For a given synthetic test containing N_E events, all with the same SNR, each detector produces N_F false alarms and N_D detections of which N_C are correct. Then

$$P_D = \frac{N_C}{N_E}$$

$$\text{FAR} = N_F \cdot \text{length of data set}/\Delta t .$$

By repeating the test with events covering a range of signal-to-noise ratios, a family of curves, similar to the single ROC sketched in Figure 1.2, may be formed.

A reasonable way to compare various detection algorithms is to test them against the theoretical "best" detector. Suppose that the seismological problems were completely solved and the signal and arrival time were perfectly known. Then the detection algorithm would have to choose between

$$X(t) = N(t) \quad \text{hypothesis } H_0$$

and

$$X(t) = S(t) + N(t) \quad \text{hypothesis } H_1$$

where $S(t)$ is completely known. Surely, we cannot expect to do better than this.

Helstrom (1968) shows that in this case, a monotonic function of the likelihood function is

$$G = \int_0^T q(t) X(t) dt \quad (1.17)$$

where T is the detection window and $q(t)$ is a solution of

$$S(t) = \int_0^T q(u) \phi(t-u) du \quad (1.18)$$

where $\phi(t-u)$ is the covariance of the stationary gaussian noise $N(t)$. The expected values of G under the hypotheses are

$$E(G/H_0) = 0$$

$$E(G/H_1) = \int_0^T q(t) S(t) dt \equiv d^2$$

The variance is the same under both hypotheses

$$\begin{aligned} \text{Var } G &= \int_0^T \int_0^T q(u) q(t) E [N(u) N(t)] du dt \\ &= \int_0^T q(t) S(t) dt = d^2 \end{aligned} \quad (1.19)$$

by equation 1.18 above. The p.d.fs of the detection statistic are

$$P_0(G) = \sqrt{2\pi d^2} \exp [-G^2/2d^2]$$

$$P_1(G) = \sqrt{2\pi d^2} \exp [-(G-d^2)^2/2d^2]$$

and the false alarm and detection probabilities are

$$Q_0 = \text{erfc}(G_0/d)$$

$$Q_1 = 1 - \text{erfc}(d-G_0/d) \quad (1.20)$$

where G_0 is the decision level of the statistic G .

The parameter d is in fact the true signal-to-noise ratio. The easiest way to see this is to consider the case where the signal $S(t)$ is zero outside the interval 0 to T . Then

$$S(t) = \int_{-\infty}^{\infty} q(u) \phi(t-u) du$$

Then taking Fourier transforms and using the convolution theorem

$$Q(\omega) = \frac{S(\omega)}{\phi(\omega)}$$

and

$$q(t) = \int_{-\infty}^{\infty} \frac{S(\omega)}{\phi(\omega)} e^{i\omega t} \frac{d\omega}{2\pi}$$

Then equation 1.19 becomes

$$\begin{aligned} d^2 &= \int_{-\infty}^{\infty} \left[\int_{-\infty}^{\infty} \frac{S(\omega)}{\Phi(\omega)} e^{i\omega t} \frac{d\omega}{E\pi} \right] S(t) dt \\ &= \int_{-\infty}^{\infty} \frac{|S(\omega)|^2}{\Phi(\omega)} d\omega \end{aligned}$$

which is simply the integral of the signal Fourier spectrum divided by the noise power spectrum.

Plots of Q_d versus d for various Q_0 and Q_d versus Q_0 for various d (the receiver operating characteristics) are given in Figures 1.5 and 1.6.

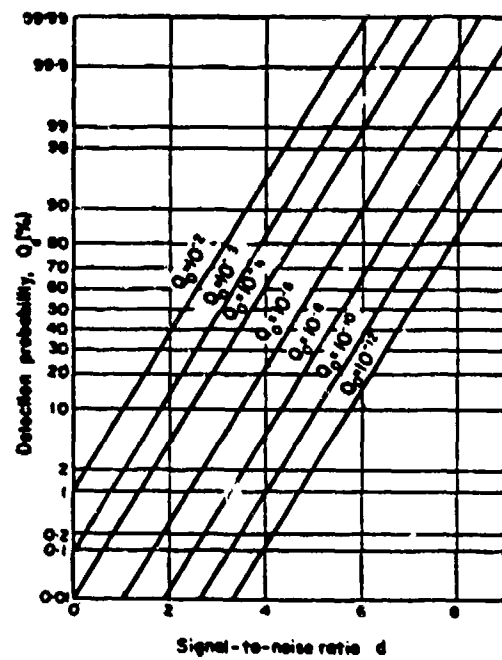


Figure 1.5 Probability of detection: completely known signal (after Helstrom, 1978, p. 106).

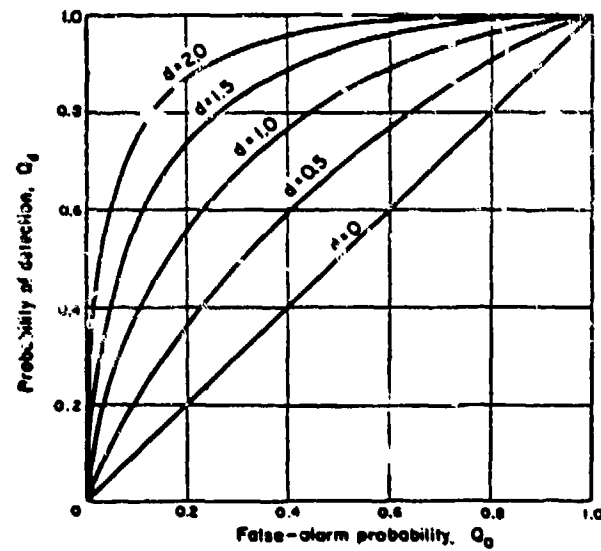


Figure 1.6 Receiver operating characteristics: completely known signal (after Helstrom, 1978, p. 197).

II. IMPORTANT SEISMIC EVENT DETECTORS

We review in this section eight seismic detection algorithms which have been developed and tested by various organizations over the past 15 years. Specifically, these are:

1. The IBM detector.
2. The Z detector.
3. The deflection detector.
4. The analytic envelope detector.
5. The Allen detector.
6. The Stewart detector.
7. The Walsh detector.
8. The MARS detector.

Most of these have been developed for the detection of teleseismic signals recorded by short period seismometers. Much of the early work was stimulated by the deployment of the LASA and NORSAR large aperture seismic arrays but more recently emphasis has been placed on developing detection algorithms to operate on single traces at the seismometer location. Such detectors have been implemented on the SRO seismometers and several small portable seismic recording systems. In these latter applications, implementation is often made on a microprocessor and so execution speed and algorithm simplicity are at a premium.

In the following descriptions of the detection algorithms, we have depended heavily on the reference given at the beginning of each subsection. Unless otherwise stated, text enclosed in quotes is taken from these reports. In the references section at the end of Section IV, all quoted literature is listed along with the abstracts of the principal works. In Appendix A, a more complete bibliography is to be found.

2.1 IBM DETECTOR, VANDERKULK, et al. (1965)

This report describes the seismic detection algorithm developed in 1965 by IBM for use on the LASA array and subsequently implemented at

NORSAR. The LASA array consisted of 525 seismometers grouped into 21 sub-arrays of 25 seismometers each. The computer system used for detection has as its input some 300 beam outputs, the subarray vertical beams, and the outputs from 21 single seismometers (one from each subarray) attenuated to record large signals.

"The processing applied to a single LASA beam output can be described as a filtering process designed to de-emphasize those frequency components where the beam output signal-to-noise ratio is low compared to its maximum. The filtering process is followed by an integration operation in which either the square or the magnitude of the filtered beam channel is integrated over a time interval of fixed duration. The resulting single quantity must then be compared with a threshold value for detection purposes."

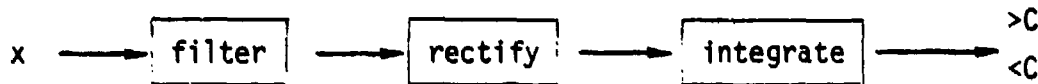


Figure 2.1. The IBM detector.

This detector, schematically represented by a flow diagram in Figure 2.1, is quite close to the one prescribed by Frieberger (1963) as described in Section 1.2, except that:

1. The filter used was not the optimum filter,

$$\sqrt{\frac{F_S(\omega)}{F_N(\omega)[F_S(\omega) + F_N(\omega)]}}$$

but simply $\sqrt{1/F_N(\omega)}$ which is the large SNR limit of the optimum; (In fact, according to Blandford (1980 Private Communication), IBM did not use an adaptive filter or even a $1/F_N(\omega)$ filter but merely a bandpass.)

2. The absolute value of the filter's output was taken for computational efficiency (speed) rather than the square;

3. The integrator was a "leaky" integrator implemented by a digital recursive filter rather than a proper integrator.

Vanderkulk (1964) examined the effects of these three approximations.

The filter with an amplitude response of $1/\sqrt{F_N(\omega)}$ was applied only over a band $\omega_1 \leq \omega \leq \omega_2$ and zero outside. The phase was arbitrary. To gauge the effects of such a filter, the report assumed that $F_S(\omega)/F_N(\omega)$ peaked at frequencies ω_0 in the center of the band and fell off exponentially on either side so the ratio was L db below the peak at ω_1 and ω_2 .

"Figure 2.2 depicts the graph of the loss versus L. As could be expected, the graph shows a minimum: when L is small, the performance of the noise-prewhitening filter suffers because too little of the signal is passed; when L, and hence the bandwidth, is large, the performance deteriorates because the filter passes too much noise."

Note that the loss in performance is less than 1 db when L is between 2.2 db and 12 db. Thus, to assure a loss of less than 1 db, the noise-prewhitening filter bandwidth must be large enough to include all frequencies where the input signal-to-noise ratio is within 2.2 db of its maximum, but must reject all frequencies where the signal-to-noise ratio is more than 12 db below the maximum. Thus, in practice, a comfortable frequency margin is allowed in which to achieve the filter cutoff. The above result permits another interpretation as well. It shows that those frequency components of the input channel where the signal-to-noise ratio is more than 2.2 db below the peak value are ineffective so far as signal detection is concerned. Therefore, the signal processing which produced the input channel is allowed to be arbitrarily degraded for those frequencies where the signal-to-noise ratio is more than 2.2 db below the maximum, so long as the signal-to-noise ratio in the region where it is within 2.2 db of the maximum is not materially altered."

The effect of rectifying rather than squaring the output of the prefilter was also investigated in this report.

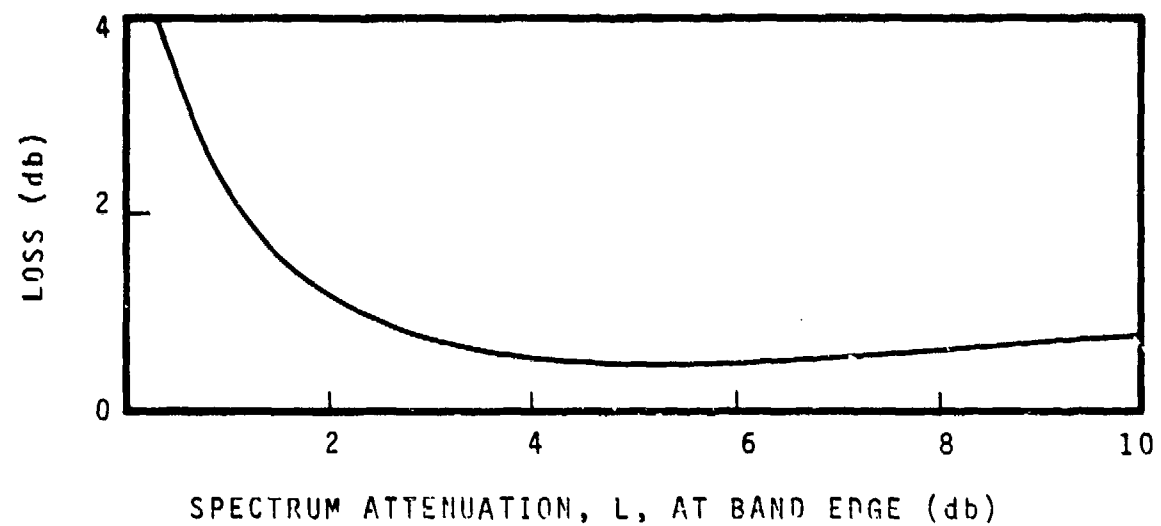


Figure 2.2. Loss in performance of the noise-prewhitening filter
for the IBM detector (after Vanderkulk, et al., 1965).

"When rectifying and integrating, the output produced is given by

$$R = \frac{1}{T} \int_0^T |x(t)| dt . \quad (2.1)$$

When squaring and integrating, the output is given by

$$P = \frac{1}{T} \int_0^T x(t)^2 dt . \quad (2.2)$$

The channel trace, $x(t)$, is assumed to be the sum of Gaussian stationary signal (when present) and Gaussian stationary noise. The loss incurred by applying rectified integration instead of squaring and integrating is found by dividing the signal-to-noise ratio of P by that of R "The resulting quotient, Q , is given by

$$Q = \frac{1 + \sqrt{1 + (S/N)}}{2} A , \quad (2.3)$$

where

$$A^2 = \frac{(\pi - 2) \int_0^T \int_0^T \hat{\rho}(t_2 - t_1) dt_1 dt_2}{\int_0^T \int_0^T \rho(t_2 - t_1)^2 dt_1 dt_2} , \quad (2.4)$$

in which formula $\rho(t_2 - t_1)$ designates the correlation coefficient between $x(t_1)$ and $x(t_2)$ when noise alone is present, and $\hat{\rho}(t_2 - t_1)$ designates the correlation coefficient between $|x(t_1)|$ and $|x(t_2)|$ when noise alone is present. Furthermore, S is the total signal power, i.e.,

$$S = \int_0^\infty S(f) df . \quad (2.5)$$

Likewise, N is the total noise power. Thus, S/N may be termed the input signal-to-noise power ratio.

It is readily shown that

$$\hat{\rho} = \left(\rho \arcsine \rho + \sqrt{1 - \rho^2} - 1 \right) / \left(\frac{\pi}{2} - 1 \right) , \quad (2.6)$$

from which it follows that

$$\rho^2 / (\pi - 2) \leq \hat{\rho} \leq \rho^2 . \quad (2.7)$$

Consequently, $1 \leq A \leq \sqrt{\pi - 2} \approx 1.07$. Since the loss in performance is $10 \log_{10} Q$ db, this loss is given by the following expression:

$$\text{Loss} \approx 10 \log_{10} \left[\frac{1 + \sqrt{1 + (S/N)}}{2} \times 1.035 \right] \text{db} , \quad (2.8)$$

where the error due to equating A to 1.035 is less than 0.2 db." For this model the loss in performance is not significantly affected by the shape of the noise spectrum or by the choice of the integration time T . A graph of the loss versus the input signal-to-noise ratio S/N is shown in Figure 2.3.

Finally, the effects of the leaky integrator were examined. Most of the detectors that are implemented using sampled data use recursive filters to simulate integrators. Typically, the output Y_i at time t_i is given by

$$Y_i = (1 - C)Y_{i-1} + C X_i \quad (2.9)$$

where C is a constant < 1 and X_i is the input. In matrix notation this can be approximated by

$$\underline{Y} = \alpha \underline{M} \underline{X} \quad (2.10)$$

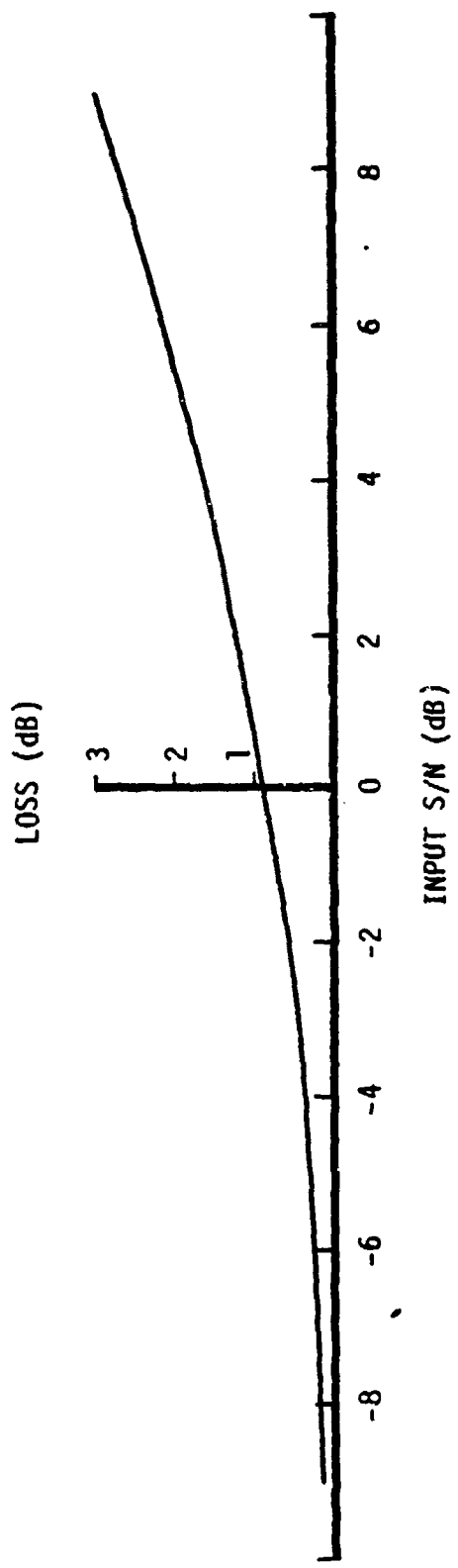


Figure 2.3. Loss in performance caused by rectifying rather than squaring the prefilter output
(after Vanderkulk, et al., 1965).

where

$$\underline{M} = \begin{vmatrix} 1 & 0 & 0 & 0 & 0 & \dots \\ (1 - C) & 0 & 0 & 0 & 0 & \dots \\ (1 - C)^2 & (1 - C) & 1 & 0 & 0 & \dots \\ (1 - C)^3 & (1 - C)^2 & (1 - C) & 1 & 0 & \dots \\ \vdots & \vdots & \vdots & \vdots & \vdots & \dots \\ \vdots & \vdots & \vdots & \vdots & \vdots & \dots \end{vmatrix} \quad (2.11)$$

The exponential integrating filter output can be represented by

$$Y = \int_{-\infty}^t x(u)^2 \exp\left(-\frac{t-u}{T}\right) du, \quad (2.12)$$

while the straightforward power integration is given by

$$Z = \int_t^{t+T} x(u)^2 du. \quad (2.13)$$

In order to assess the effect of finite signal duration, the signal is taken to be a portion of duration T_s of a Gaussian stationary process. It follows that optimum processing (maximized signal-to-noise ratio) is produced by using the output Z with $T = T_s$ and with the interval from t to $t + T_s$ exactly covering the signal time interval.

With this maximum possible signal-to-noise ratio as a standard, the loss in performance resulting from the use of the exponentially decaying integrating filter (with T being arbitrary) is given by the following expression:

$$\text{Loss} = -10 \log_{10} \left[\sqrt{2} \sqrt{\frac{T}{T_s}} \left(1 - \exp(-T_s/T) \right) \right]. \quad (2.14)$$

This formula was obtained by computing the quotient of the maximum possible signal-to-noise ratio and the signal-to-noise ratio of the rectified integration output Y , with t being the endpoint of the signal time interval. The loss is then equal to 10 times the logarithm of this quotient. The preceding formula for the loss is an approximation obtained by assuming that both T_s and T are large compared with the reciprocal of the noise bandwidth (or, equivalently, compared with the decay time of the noise autocorrelation function $\rho(t)$). Figure 2.4 is a graph of the loss versus T/T_s . The minimum loss occurs when $T = 0.80 T_s$ and is 0.45 db. The performance loss is less than 0.55 db when T lies anywhere between $0.55 T_s$ and $1.10 T_s$. Thus, by tolerating this loss, it is sufficient to implement this exponentially decaying, integrating filter with a sequence of filter decay times T which progresses by factors of two.

The separate performance loss considerations given above should more properly have been combined to provide the simultaneous effect of these three factors on the signal processing performance.

The only difference between the "IBM" detector and the conventional power detector (see Section 1.2) is that the former takes the positive square root of x_i^2 (i.e., the absolute value, a computationally efficient quantity) rather than the square. As we saw earlier, under a simple model of the noise signal, the loss in performance caused by taking $|x_i|$ instead of $|x_i^2|$ is only about 1 db (0.05 m_b difference in detection capability).

The IBM approximation to the conventional power detector is basically the algorithm that is used at both NORSAR and SDAC.

The data sampled at 20 sps is first decimated (without filtering) to 10 sps. The data is next passed through a recursive band pass filter and further decimated to 5 sps. This is the input data stream to the rectifier (absolute value)

$$Y_i = |x_i| \quad \text{where } \Delta i = 0.2 \text{ sec.} \quad (2.15)$$

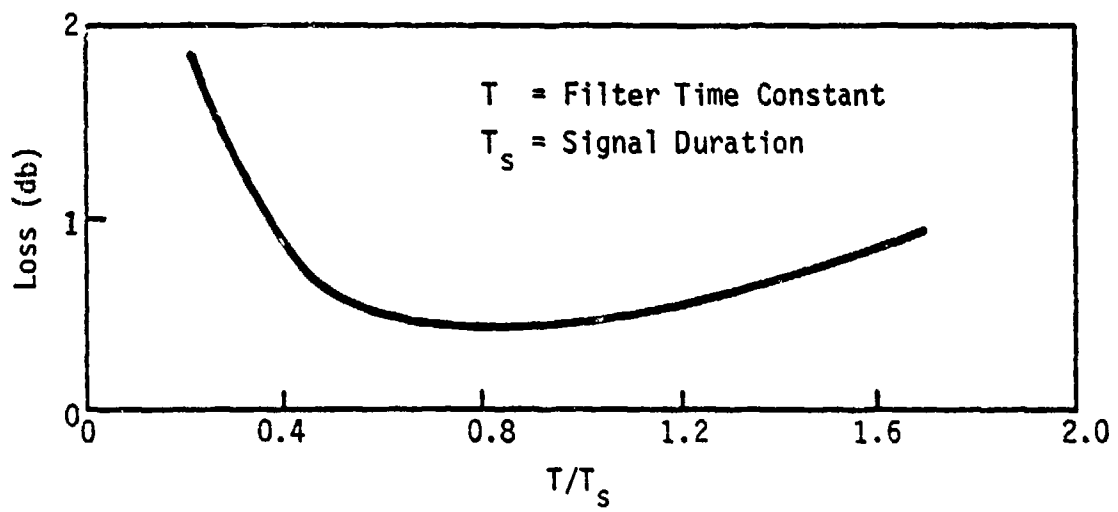


Figure 2.4. Performance loss of an exponential integrating filter
(after Vanderkulk, et al., 1965).

these rectified quantities are then averaged into groups of three

$$\bar{Y}_i = \frac{1}{3} \sum_{j=i-2}^i |x_j| \quad \text{where now } \Delta_i \text{ corresponds to } 0.6 \text{ sec, i.e., a decimation by 3.} \quad (2.16)$$

The three-point averages are then further averaged over three 0.6 second intervals (1.8 second) (i.e., no decimation) to form the STA, which is updated every 0.6 second.

$$STA_i = \frac{1}{3} \sum_{j=i-2}^i \bar{Y}_j \quad \begin{aligned} \Delta_j &\text{ corresponds to 0.6 sec} \\ \Delta_i &\text{ corresponds to 0.6 sec} \end{aligned} \quad (2.17)$$

The long-term average, LTA, is formed by a first-order recursive filter acting on the 0.6 second samples of the STA. However, there is a further decimation by three so that the LTA filter output is derived from statistically independent samples of the STA

$$LTA_i = (1-C) LTA_{i-1} + C STA_{3j} \quad \begin{aligned} \Delta_j &\text{ corresponds to 0.6 sec} \\ \Delta_i &\text{ corresponds to 1.8 sec} \end{aligned}$$

Typically, C is set for a 30 second time constant: (2.18)

$$C = \frac{\Delta t}{T_i} = \frac{1.8}{30} = 0.06. \quad (2.19)$$

The decision algorithm examines the 0.6 second samples of STA and compares this to the 1.8 second samples of the LTA. If

$$STA > K * LTA \quad (2.20)$$

for Q out of Q' successive tests an event is declared. Typically Q/Q' is set at 2/3 or 3/3 and K is approximately 3. Note that since LTA is only updated every 1.8 second, it remains constant over this test.

When an event is declared, the time constant of the LTA recursive filter is reduced typically to half its normal value until the event is declared over. This is done to detect the later phases.

2.2 "Z" DETECTOR, SWINDELL AND SNELL (1977)

The "Z" detector was the result of research to develop a constant FAR (CFAR) algorithm for the Station Processor. This "detector is a modification of a conventional power detector which detects signals as short-term-averaged (STA) signal power relative to long-term-averaged (LTA) noise power preceding the signal. Statistical analyses of STA noise fluctuations indicated that small deviations in the STA standard deviation from LTA causes serious problems in controlling false alarms. This sometimes leads to the unstable operation of conventional power detectors. In some cases, such instability causes the detector to turn on or to shut off for long periods of time. The "Z" detector was designed to solve this problem by continuously adjusting the threshold of STA-LTA to a fixed number of standard deviations of STA-LTA. Estimates of the standard deviation are updated on a point-by-point basis. The "Z" detector is also designed to control false alarms from the coda of large signals." Basically, the detector statistic for noise input was modeled as a log-normal process. The mean and variance of the statistic were used to transform the statistic to a zero-mean, unit variance quantity called the "Z" statistic. Thus, for a single random variable x , the Z statistic is defined as

$$Z(x) = \frac{x - \mu(x)}{\sigma(x)} . \quad (2.21)$$

The idea for the logarithmic transformation came originally from LaCoss's (1972) observation that the STA values from the IBM detector looked to be normal distributed. Of course, if the input signal were Gaussian, and the STA values were a true estimate of the power, they would be χ^2 distributed. This distribution, for a small number of degrees of freedom, is not unlike a log normal distribution in appearance. However, as the IBM STA algorithm does not, in fact, estimate power, but rather averages the absolute value, LaCoss's empirical approach to the correct distribution is reasonable.

In any event, the "Z" detector proceeds as follows:

1. The input data are band passed with a recursive filter. This filter is centered at about 2 Hz and is between

3 and 4 Hz wide. The principal purpose of the filter is to remove the mean from the data. It is not chosen "a la Frieberger" to optimize detectibility.

2. The beginning operation for the detection statistic is a squaring rather than rectifying operation

$$Y_i = x_i^2 . \quad (2.22)$$

3. As in the NORSAR/SPAC implementation of the conventional power detector, the Y_i are averaged over some gate N by

$$\bar{Y}_j = \frac{1}{N} \sum_{i=j-N}^j Y_i . \quad (2.23)$$

The time interval associated with \bar{Y} is N times longer than that associated with Y . M sets of these points are then averaged to form the STA which yields

$$STA_k = \sum_{j=k-M}^k \bar{Y}_j \quad (2.24)$$

STA is updated just as frequently as \bar{Y} .

4. "The logarithm of the short-term average, STA, is passed to the long-term background level estimator to be used for updating the long-term estimate, μ , of log STA and of the variance σ^2 , of log STA. Z is computed using μ and σ before they are updated with the present value of log STA. Then a sequential threshold test is performed. The first test compares the absolute magnitude of z to the threshold value of z , z_{TH} . This is to prevent the LTA from updating either on true detections (positive z) or highly negative values of z arising from the logarithm of very low powers which

occur momentarily. If the threshold is exceeded, the sign of z is checked and, if positive, a detection is declared."

5. The fifth step is a detection analyzer which "suppresses multiple declarations of detections from the same signal caused by coda levels continuously exceeding the detection threshold, posts new detection declarations if coda levels show unusual increases in level, and controls the LTA estimator to prevent LTA estimates from being contaminated by coda energy."

The concept of a post detection processor, found in other detectors as well, is important. It allows one to build a "front end" system that is fast, which has a large FAR, but which culls the data stream to a more manageable volume. In the "Z" detector, "the internal logic of the analyzer is moderately complicated and is best understood by its action on a typical signal (see Figure 2.5). It may be broken down further into a coda suppressor and LTA controller.

When the input z crosses the threshold z_{TH} , the time is noted and a timer is initiated. After the specified time, the beam select gate, has elapsed, the detection time and the peak value of z occurring in this gate is stored for the beam selector's use. The beam selector gate is operator adjustable and typically lasts ten seconds. Also at the detection time, a second timer is initiated which defines a secondary detection gate. (This gate is also operator adjustable; during this study, 15 seconds was used.)

Assume for the moment that the signal is small and the coda level drops below the threshold a few seconds after the initial detection. The situation now is: no detections are occurring at the z comparator, there is remnant signal coda energy present, but it is decaying toward the original noise level. When z becomes less than z_{TH} , a third timer, also operator adjustable, is initiated which defines the detector reset time. After this time has elapsed, the detector is reset and any new threshold crossing will be declared a new detection. For this study, a reset time of 20 seconds was used. The purpose of the reset time is to prevent new detections from being declared because of "jitter" in the

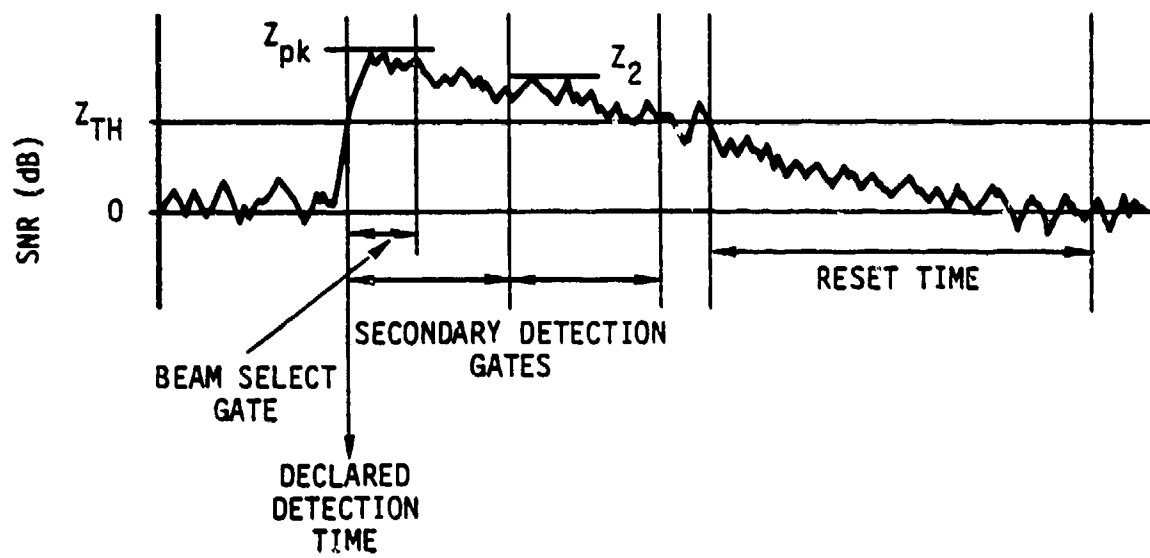


Figure 2.5. Coda suppressor for the "Z" detector (after Swindell and Snell, 1977).

z values as they decay through the threshold. The reset time must be greater than the secondary detection gate which in turn is greater than the beam selector gate.

The reaction to a large signal where z remains above z_{TH} for at least two secondary detection gate intervals is slightly more elaborate. The goal is to monitor the coda level for the arrival of secondary phases or signals from another event. The operating assumption is that the coda level will decay fairly smoothly from its initial peak except when new signals arrive. As each secondary detection gate lapses (except the first one), the peak z in that gate is compared with the peak value from the preceding gate. If it exceeds the old peak by some specified amount (e.g., 6 dB, operator adjustable) than a new detection is declared.

The LTA controller maintains the highest level of control of the LTA estimator and its job is to exclude as much signal-related energy as possible from the estimates of the mean and standard deviation of the log STA for the background noise. Its action can also be described more easily by example (refer to Figures 2.6 and 2.7). After computing z , the LTA estimator normally updates μ and σ^2 with every new datum except when inhibited. The threshold comparator issues an inhibit command whenever $|z| > z_{TH}$. Finally, to insure that a very large signal does not keep μ frozen too long the freeze time is limited to some maximum, say 10 minutes, which is also operator adjustable. When μ becomes unfrozen by any means, it assumes the present value of LTA and normal updating resumes. Internal to the LTA estimator, there are actually two separate estimates of mean and standard deviation of log STA. Using the mean as an example (the σ^2 estimate follows in parallel), the two quantities are μ and "LTA". Z is always computed using μ .

Under conditions of noise with no inhibiting commands from the LTA controller, μ and LTA are identical. When a detection occurs, the dichotomy of LTA and μ becomes apparent. Whenever $|z| < z_{TH}$, LTA updates but μ remains frozen at least until the LTA reset time interval

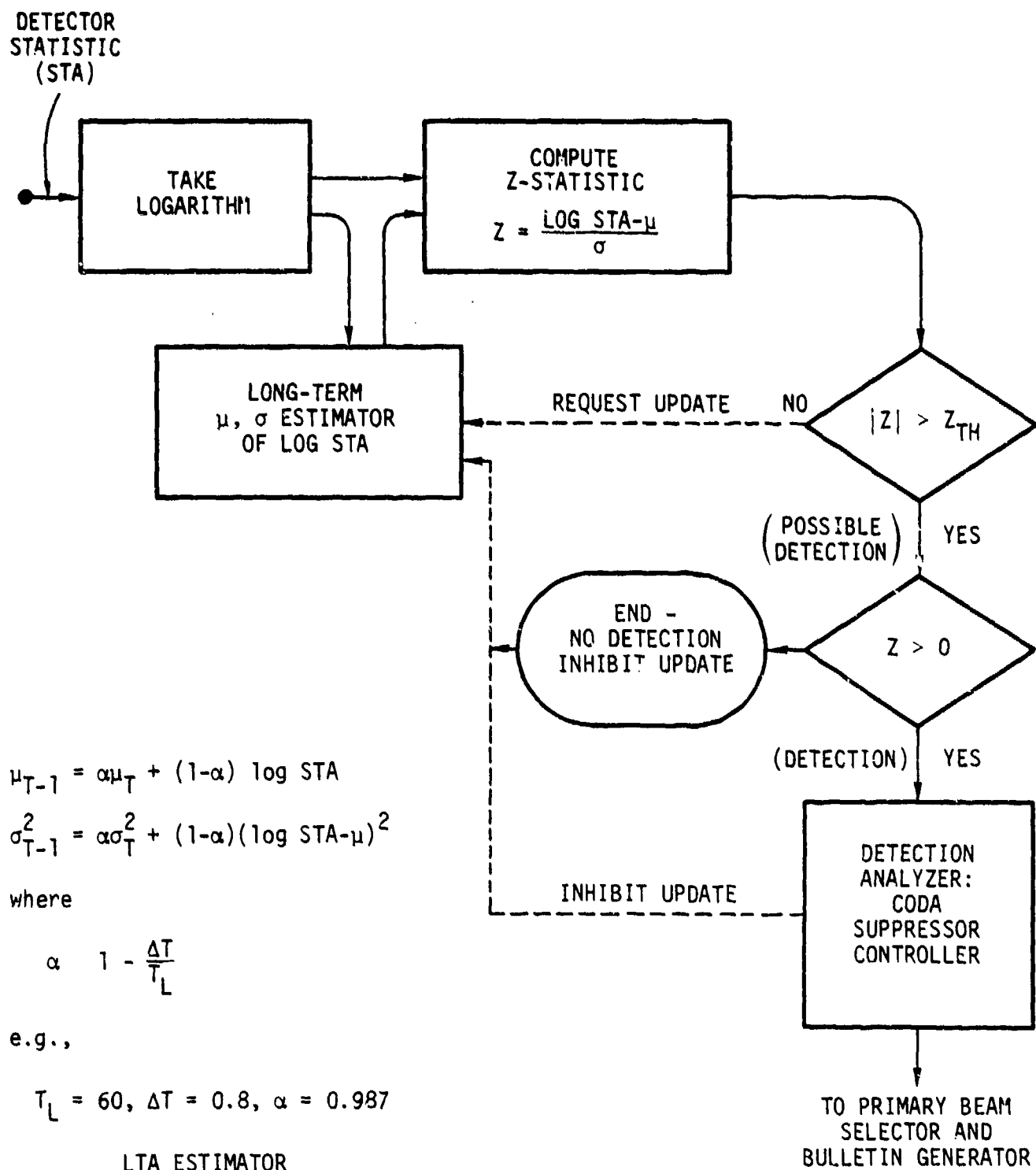


Figure 2.6. "Z" detector flow diagram (after Swindell and Snell, 1977).

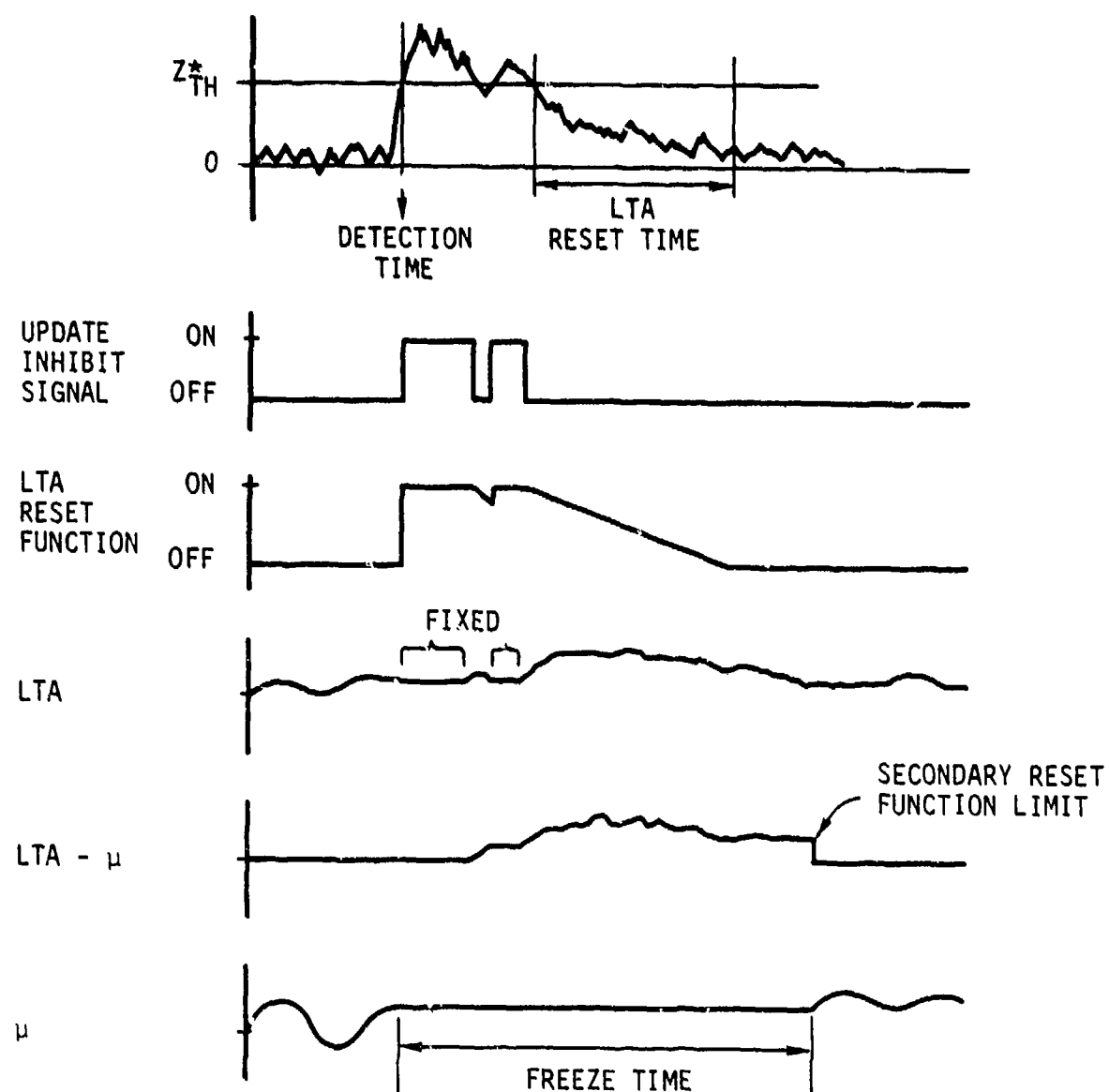


Figure 2.7. "Z" detector LTA controller (after Swindell and Snell, 1977).

has elapsed. At the end of the reset time a test of the difference between LTA and μ is made and μ remains frozen until that difference becomes small enough. This maximum difference is called the secondary reset function limit and is operator adjustable."

Evaluation of the "Z" detector was reported in Swindell and Snell (1977) using data from the KSRS array during different periods of the year. They concluded that "the Z statistic algorithm produces a constant false alarm rate rather than a constant alarm rate and is essentially independent of the noise field behavior. The estimated mean and variance of the noise which is used to convert the basic detector output to Z also provides information useful for estimating station performance as part of a network and makes unnecessary a separate noise level calculation for the power detector. Alarm rates may be set independently for each beam (signal) to reflect differences in seismicity or to give some beams (signals) higher sensitivity without affecting overall alarm rate."

They also tested two different pre-detection band pass filters and concluded that they caused no appreciable differences on the outcome, nor did changes in the integration time of the STA process from 1.6 second to 3.2 seconds have appreciable effect.

Further tests of this automatic detector were conducted during two months of field operation at DET 459 by Secoy (1978). Sax (1980) reports that "at KSRS, 70 percent of the analyst picks were automatically detected with 0.875 false alarms per hour and with a stability of about 35 percent. At DET 459, 70 per cent of the analyst picks were automatically detected with 0.375 false alarms per hour. These false alarm figures are on a per-beam basis so that they are comparable with those expected for a single-sensor channel. The timing accuracy of the detector indicated a late bias of 1.7 seconds, with a standard deviation of 2.2 seconds.

The potential exists for making major improvements in the "Z" detector. A need exists to reduce false alarms caused by local seismic signals, and to provide a restart mechanism for automatically "warming-up" the detector after long power outages. Also, there is a need to provide post-detection processing in order to improve the timing accuracy

of signals, and possibly to cope with multiple arrivals of complex and multipathed signal transmissions. A recent application of the "Z" detector by Sax, et al. (1979b) indicates that the detector at KSRS provided precise magnitude estimates of complex events from a selected USSR border region. Timing associated with event arrivals, in this case, was complicated by the repeated arrival of other events, at equal perceived magnitudes, for up to a minute following the first arrival.

Additional work is needed to develop pre-filters to optimize the detection of earthquakes and explosions. Since the signal-to-noise ratio (SNR) for explosions and local events may be significantly different from that for earthquakes, it may be desirable to provide more than one optimized pre-filter for more complete extraction and identification of various signal types.

2.3 DEFLECTION DETECTOR, SHENSA (1977)



The deflection detector works in the Fourier domain by taking data vectors \underline{x} and calculating the digital Fourier transform of that data set. Using an FFT algorithm, the power $P_i(k)$ (for each frequency k , $P_i(k)$ is the real part of the FFT squared plus the imaginary part of the FFT squared) at the k^{th} frequency is found for the i^{th} epoch or time window. This moving power spectrum estimator is used in three closely related detectors (see Figure 2.8):

1. The average (or stacked) power detector.
2. The maximum deflector detector.
3. The average (or stacked) deflection detector.

In each of these cases, Shensa (1977) used both $P_i(k)$ and $P_i'(k) = \log P_i(k)$ as the basic input quantity, but in all cases he found that taking the logarithm decreased the probability of detection for a given SNR.

2.3.1 The Average Power Detector

This detector is simply the "Z" detector operating in the frequency domain. The average of $P_i(k)$ over some signal band is found and a Z-statistic calculated by normalizing to the mean and standard deviation of the average power

$$Y_i = \frac{\frac{1}{N} \sum_{k=N_1}^{N_2} P_i(k) - \mu}{\sigma} \quad N = N_2 - N_1 \quad (2.25)$$

where μ and σ are the mean and standard deviation of the average power.

This is really an estimate of

$$\frac{Var_i - \mu(\text{var})}{\sigma(\text{var})}, \quad (2.26)$$

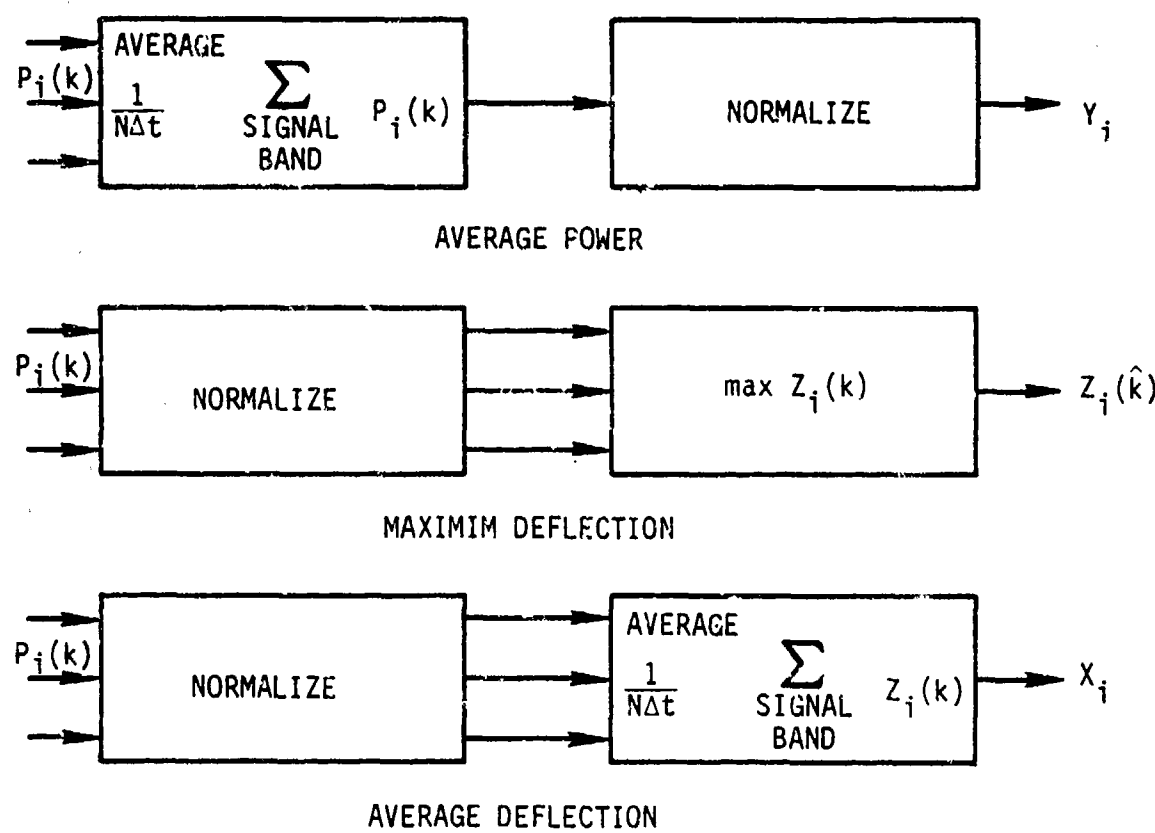


Figure 2.8. Block diagram of three deflection detectors showing how the scalar statistic X , Y or Z is derived from the power spectrum $P_i(k)$ (After Shensa, 1977).

or simply a

$$\frac{\text{STA(var)} - \text{LTA(var)}}{\sigma(\text{var})} , \quad (2.27)$$

which is just what Swindell and Snell (1977) calculated in the time domain for the "Z" detector, after taking the log of the short term variance estimator. An event is declared if this ratio exceeds some fixed threshold.

2.3.2 The Maximum Deflector Detector

The power $P_i(k)$ is converted into a "Z-statistic" on a frequency-by-frequency basis by the usual transformation

$$Z_i(k) = \frac{P_i(k) - \mu(k)}{\sigma(k)} \quad (2.28)$$

where $\mu(k)$ and $\sigma(k)$ are the mean and standard deviation of the power at the k^{th} frequency calculated in the absence of a seismic signal. At each epoch (value of i) the maximum $Z_i(k)$ is compared against a fixed threshold value and an event declared if it exceeds this value.

2.3.3 The Average Deflection Detector

In this detector, instead of choosing the $\max [Z_i(k)]$ the average across some band is used

$$x_i = \frac{1}{N} \sum_{i=N_1}^{N_2} Z_i(k) \quad \text{where } N = N_2 - N_1 \quad (2.29)$$

With this implementation, the standardized variable Z_i is computed on a frequency band-by-frequency band basis. There is a certain simplification by noting that for the unsmoothed spectral estimators used here, the standard theory of random data analysis yields the result that in the absence of signal the sampling distribution of $P_i(k)$ is given by

$$P_i(k) = x_2^2 \frac{\tilde{P}_i(k)}{2} \quad (2.30)$$

where χ_2^2 is the chi squared random variable with two degrees of freedom, and $P_i(k)$ is the true power spectral density. Since

$$E[\chi_2^2] = 2$$

$$\text{Var} [\chi_2^2] = 4$$

we see

$$\mu \approx \tilde{P}_i(k) ,$$

$$\sigma \approx \tilde{\sigma}_i(k) .$$

This is the well known result that in the absence of smoothing, the standard derivation of a power estimate equals the estimate itself. Thus, equating the LTA with μ for each frequency, we get

$$Z_i(k) = \frac{\text{STA}(k)}{\text{LTA}(k)} - 1 . \quad (2.31)$$

Although $P_i(k)$ is itself χ_2^2 distributed, the statistic on $Z_i(k)$ is not so simple because, of course, μ and σ themselves are not known exactly but must be estimated from the data.

This detector statistic is proportional to a weighted power spectral density average between N_1 and N_2 . In contrast with the average power detector, the average deflection detector weights each power spectral density component inversely with the estimated standard deviation of the noise power spectral density. The detection statistic used produces the same incoherent noise gain as the average power detector, but it is optimum only for independent spectral noise fluctuations. The average deflection detector differs significantly from the average power detector in that it weights the signal spectrum more heavily at those frequencies where it peaks relative to the noise spectrum. Note the similarity between this and the $\sqrt{1/F_N(\omega)}$ prefilter of the IBM detector (Section 2.1), and the prewhitening operation of the Walsh detector (Section 2.7).

Several weak-signal scenarios are given to illustrate factors which influence the comparative performance of the above three detector concepts.

The first hypothesis we shall consider is that weak signals contain energy which significantly exceeds the noise in at least one of the frequency bands monitored by the detector. In this case, the maximum deflection detector will efficiently detect such a coherent sinusoidal signal. The average deflection and average power detector would more than likely miss this type of signal since averaging over other frequency cells would reduce this signal peak by as much as $1/N$ (N frequency cells) while the incoherent gain in reducing the noise standard deviation would be no more than \sqrt{N} . Thus a detection loss as large as $1/\sqrt{N}$ from the coherent gain of the maximum deflection would result from averaging all frequencies over the full band of the detector.

A second hypothesis is that the weak signal spectrum does not exceed the noise by a significant amount in any one of the frequency bands, but it is near or slightly above the noise spectrum in the entire band covered by the detector. In this case, the maximum deflection detector would miss the signal; in addition, averaging over the band would produce a \sqrt{N} incoherent gain by the average power detector. Averaging would produce a somewhat smaller gain in the average deflection detector in that a statistically variable weighted sum would degrade the detector performance. This expected incoherent gain of \sqrt{N} would be produced by reducing the standard deviation of noise fluctuations. The latter could be accomplished by averaging the power spectral densities of the N frequency components covering the signal band.

The third hypothesis is similar to the second in that the power spectral density of the signal is near that of the noise. Consequently, no detection is possible by the maximum deflection detector because no large coherent gain can be observed at any frequency. However, in this case, the noise spectrum is unstable, and it varies greatly with statistical independence from one frequency cell to another, and also from one time slice to another. Similarly, the signal power fluctuations might

also be unstable. In either case, the weighted average of the stacked deflection detector would be required in order to achieve the most efficient detection of weak signals.

The conditions for optimum performance of the three types of spectral detectors are summarized as follows:

- The maximum deflection detector is optimized for a weak signal if the signal significantly exceeds the noise at only one or several frequencies within the signal band.
- The average power detector is an optimum detector if the weak-signal and noise spectra are stable and if the signal spectrum is near or slightly exceeds the noise spectrum uniformly over a broad range of frequencies.
- The average deflection detector is an optimum detector if the weak-signal and noise spectra are highly unstable and if the signal spectra is near or slightly exceeds the noise spectrum over a broad range of frequencies.

Shu evaluated the performance of these three detectors by adding two earthquake samples and two explosion samples to 3,000 seismic noise samples. He examined the detection performance at various input SNRs (SNRs between -6 and +9 dB). His goal was to obtain the complete operating characteristics (P_d versus P_f) for all three types of detectors. The most comprehensible results were obtained by comparing the detectors for 32-point FFTs and P_d -versus-SNR for a false alarm rate constrained at 4.5 false alarms per hour.

In the case of all four signals, the average deflection detector operating characteristics are much worse than are either the average power or the maximum deflection detector. This indicates that the seismic signal and noise spectra are nearly stable and stationary. These results also indicate that the average of spectral "Z" statistics is neither optimum nor feasible for use as a detector statistic.

In the case of the two earthquake signals, at all input SNRs, the average power detector performed best. At 4.5 false alarms per hour and for a detection probability of 0.5, the average power detector gained $0.2 m_b$ of detection capability over the maximum deflection detector in one case, and by $0.05 m_b$ in the other case. Thus, the broadband "Z" detector appears to be a superior detector of earthquakes but not necessarily of explosions. These operating results are relevant to detecting weak signals (that is, signals which are only about 6 dB above the ambient noise).

In the case of the two explosion signals and at all input signal-to-noise ratios, the maximum deflection detector performed significantly better than did the average power detector. For a false alarm rate of 4.5 false alarms per hour and a detection probability of 0.5, the detection capability gain observed was $0.17 m_b$ in one case, and $0.25 m_b$ in the other case. Shensa's results suggest that a dominant high-frequency peak in a weak explosion signal is significantly more detectable than is the result obtained when the power is averaged over a broad band of frequencies between 0.9 and 3.6 Hz. These results pertain to weak explosion signals which are nominally 4 dB above the ambient noise level.

As a step toward further optimization of spectral detectors, Shensa suggests using prior information of signal and noise spectra to perform fixed weighted estimates of the stacked power spectral density for various observed signal types (e.g., earthquakes, explosions, local events). The detector would then determine the maximum deflection from such weighted power averages as optimum detectors of events with spectra matched to previously observed signals. This suggestion is similar to that of the matched spectral pre-filters suggested for improving the broadband "Z" detector.

The computer capabilities and storage requirements needed to implement Shensa's maximum deflection detector are modest, and can probably be accomplished with a minicomputer (distributed processing is probably feasible for certain microcomputers). The programming required is only

a slightly expanded version of the broadband "Z" detector. The bulk of that program handles the suppression of redundant code detections. Therefore, the inclusion of a set of front-end filters or front-end FFTs represents only a modest program expansion. Since the maximum deflection detector reduces the spectral data down to a single value of "Z" at each point in time, the major part of the "Z" detector algorithm concerned with suppression of redundant code need only be performed once for each time slice of data.

2.4 ANALYTIC ENVELOPE DETECTOR, FARNBACH (1975); UNGER (1978)

The mathematical concept behind this detector is the representation of the signal as the real part of a complex function of time. In the simplest case this amounts to a phasor representation of a sinusoidal signal using a complex exponential instead of a sinusoid. In the case of narrow band (but not purely sinusoidal) signals, the concept is generalized to include amplitudes and frequencies that vary "slowly" with time. The advantage of this representation is the separation of amplitude and phase information which in a real signal are blended in a way which is hard to separate visually.

Any real function $f(t)$ can be extended to form the complex analytical signal (Figure 2.9)

$$C(t) = f(t) + i F_{Hi}(t) \quad (2.32)$$

where

$$F_{Hi}(t) = \frac{1}{\pi} \int_{-\infty}^{\infty} \frac{f(u)du}{u - t} \quad (2.33)$$

is the Hilbert transform. (See, e.g., Bracewell, 1965.)

If we can assign a mean frequency $\bar{\omega}$ to the signal, as we might expect for a narrow band seismic signal, then we can write the complex representation of $x(t)$ as

$$C_x(t)e^{i\bar{\omega}t} \quad (2.34)$$

where $C_x(t)$ is the generalization of the sinusoidal phasor, called the complex envelope function.

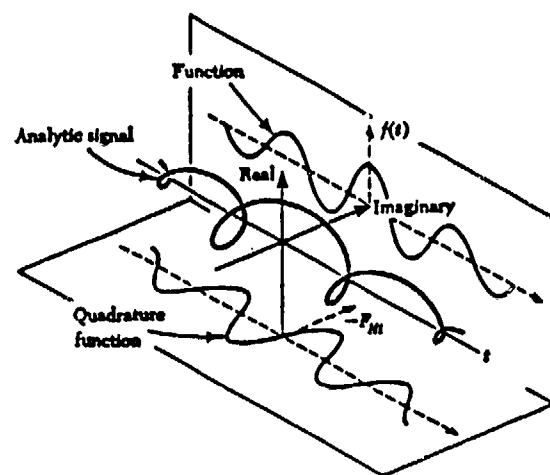


Figure 2.9. The complex analytic signal. A modulated carrier $f(t)$, its quadrature function $F_{H_1}(t)$, and the associated complex analytic signal are all shown as functions of the real variable time (after Bracewell, 1965).

$$c_x(t) = E(t)e^{i\phi(t)} \quad (2.35)$$

Then, our original signal $x(t)$ is simply the real part or

$$x(t) = E(t) \cos[\omega_0 t + \phi(t)] \quad (2.36)$$

where

$E(t)$ is the instantaneous envelope amplitude

ω_0 is the mean frequency

$\phi(t)$ is the instantaneous phase with respect to this mean frequency.

The instantaneous frequency $\omega(t)$ is given by

$$\omega(t) = \frac{1}{2} \frac{d}{dt} \phi(t) + \omega_0 \quad (2.37)$$

and

$$E(t) = [x^2(t) + x_{Hi}^2(t)]^{1/2} \quad (2.38)$$

where $x_{Hi}(t)$ is the Hilbert transform of $x(t)$.

From a practical computational viewpoint, being able to calculate the envelope function implies an associated time window or epoch. Indeed, examination of Figure 2.10 shows us that, in fact, the envelope function $E(t)$ (see Eq. (2.35)) is simply a STA of $|x(t)|$. Now, we can examine a phasor plot of the complex envelope function for a seismic waveform that is composed of a signal vector $\vec{s}(t)$ and a noise vector $\vec{n}(t)$ combining to form a resultant phasor $\vec{x}(t)$ with modulus $|x(t)|$ and phase $\phi(t)$. If we assume that the signal phase is zero, the phasor diagrams are shown in Figure 2.11, under both large signal (left frame) and small signal (right frame) conditions.

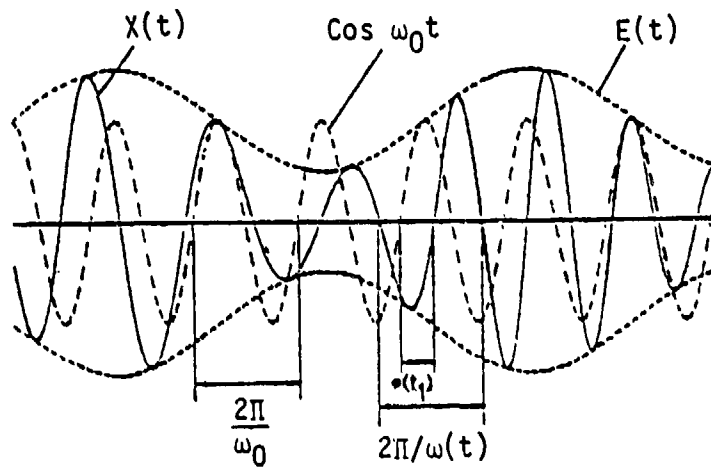
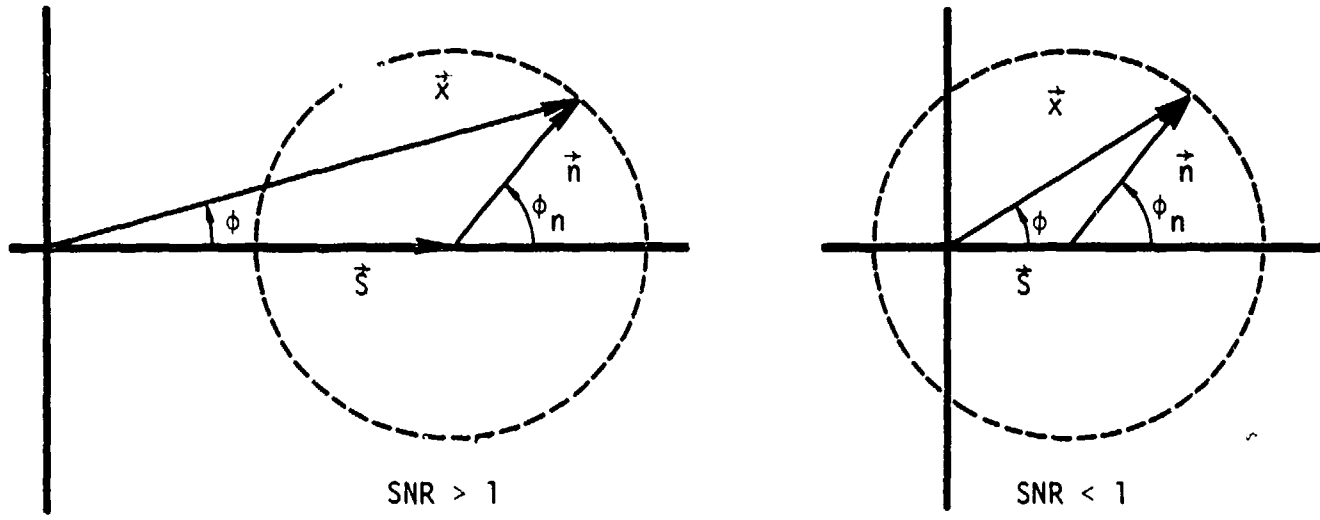


Figure 2.10. Envelope representation of the complex analytic signal
(after Bracewell, 1965).



$|\vec{r}|$ = INSTANTANEOUS AMPLITUDE

ϕ = INSTANTANEOUS PHASE

Figure 2.11. The instantaneous phasor for the complex analytic signal (after Unger, 1978).

In practice, of course, it is not possible to distinguish between the instantaneous values of $|\vec{x}(t)|$ and $|\vec{n}(t)|$. It is more useful to examine the probability that $|\vec{x}(t)| > n_0$ some long term property of the noise vector amplitude. Unger showed that if most of the time $|\vec{n}(t)| < n_0$ then

$$P(|\vec{x}_s(t)| > n_0) < P(|\vec{x}_s(t)| > |\vec{n}(t)|). \quad (2.39)$$

Thus,

$$P(|\vec{r}_s(t)| > n_0) = \epsilon, \quad s(t) = 0 \quad (2.40a)$$

$$\epsilon < P(|\vec{r}_s(t)| > n_0) < 1 - \pi^{-1} \arccos \frac{|s(t)|}{2|\vec{n}(t)|}, \quad 0 < |\vec{s}(t)| \leq |\vec{n}(t)| \quad (2.40b)$$

$$\epsilon < P(|\vec{r}_s(t)| > n_0) < 1, \quad |\vec{s}(t)| \geq 2|\vec{n}(t)|, \quad (2.40c)$$

where the ϵ is the probability that the noise envelope in the presumed signal gate is greater than n_0 in the lagging, presumed noise gate. This value depends on the statistical distribution of noise envelope values. Thus, in the presence of signal, this probability is greater than ϵ , and increases with SNR, but is subject to an upper bound which ranges from 0.5 to 1.0 as determined by the instantaneous SNR. The difference between the probability value and the upper bound increases with the difference $n_0 - |\vec{n}(t)|$. This probability distribution function is given in Figure 2.12, together with the phase bias probability distribution curve given later.

Unger (1978) described two detectors, one based on the amplitude of the envelope function and the other based on its phase.

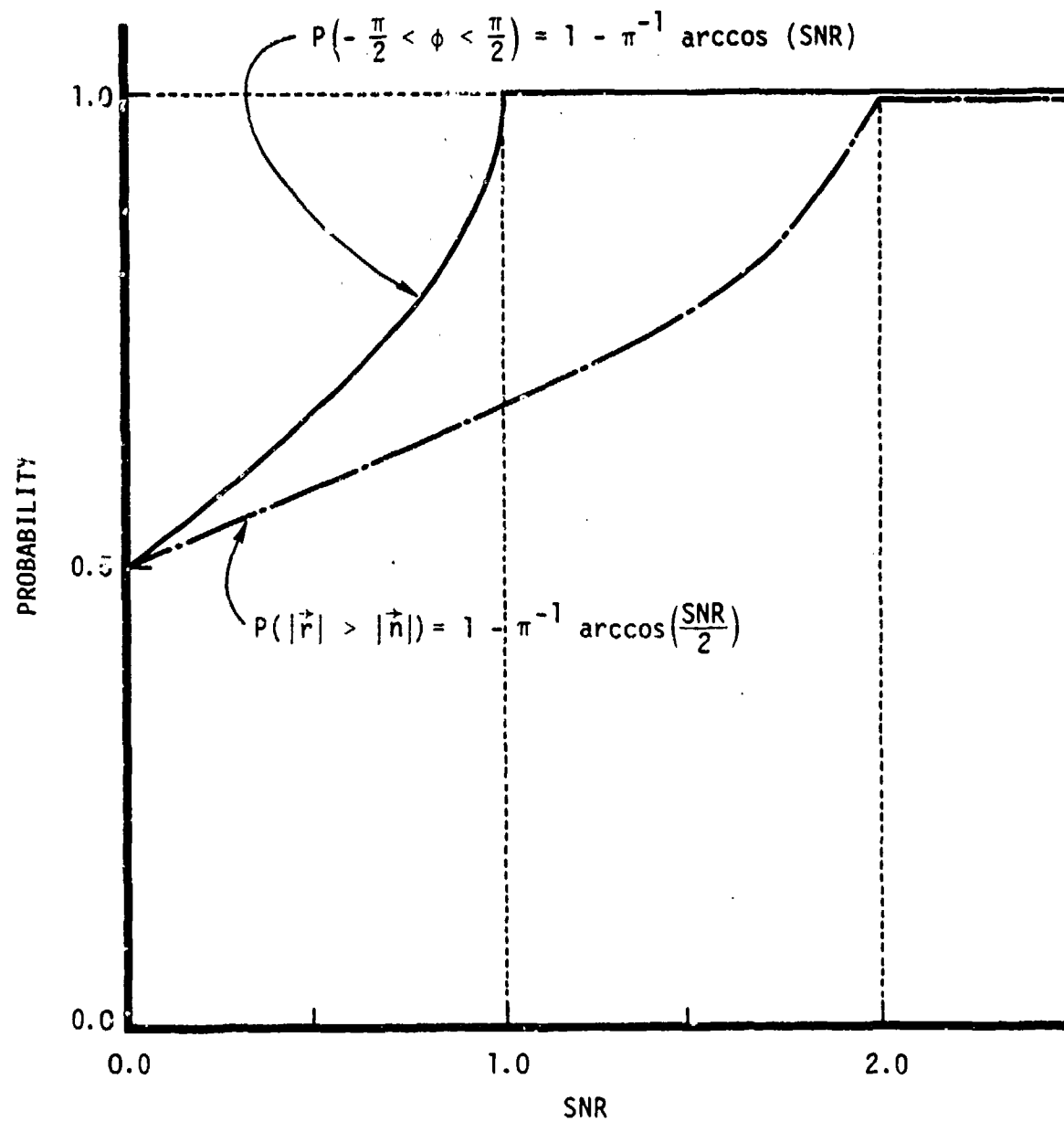


Figure 2.12. Envelope and phase probability distribution curves (after Unger, 1978).

1.0 Amplitude Detection

Unger's envelope amplitude detection algorithm used simply $n_0 = |\vec{n}|_{\max}$ over a long term noise gate and approximated the probability $P(|\vec{x}(t)| > n_0)$ by counting the number of times that, in a presumed signal gate, the envelope exceeds the maximum envelope in a lagging noise gate.

The procedure was as follows (Figure 2.13).

"First, over a specified warm-up period (e.g., 40 seconds), the peak noise envelope, $|\vec{n}|_{\max}$, is established. This peak envelope is cosine tapered over subsequent waveform points, with a specified time constant (e.g., with a 60-second time constant, the original peak value is halved at 30 seconds and equals zero at 60 seconds). An envelope value exceeding the tapered peak value establishes a new noise peak, unless a signal detection is declared; in that case no noise peak update takes place until the signal is declared to be terminated.

A signal detection is called whenever, in a forward-looking (leading) time window of specified length (e.g., 4 seconds), the probability that the envelope is greater than the tapered peak noise envelope, $P(|\vec{x}(t)| > |\vec{n}|_{\max})$ exceeds a specified threshold TH1 (e.g., TH1 = 0.3). When this probability reaches its maximum the algorithm starts looking for the first signal envelope peak. When the ratio of first signal envelope peak and tapered noise envelope peak exceeds a second specified threshold, the SNR threshold TH2 (e.g., TH2 = 2 to 3 dB), the signal detection is confirmed and a frequency-dependent stepback is performed to determine the signal onset time.

The stepback procedure (Figure 2.14) is based on the observation that in most cases the first signal envelope peak (at t_4) occurs within one signal period, and frequently at approximately 3/4 period, after the signal onset (at t_0). In a high-SNR waveform the signal onset time is most accurately found by detecting the first maximum or minimum of the signal's instantaneous value (at t_3), and stepping back 1/4 period ($= 0.25/\text{instantaneous frequency at } t_3$). For low-SNR waveforms the first quarter period may be obscured by noise; in that case we step back 3/4

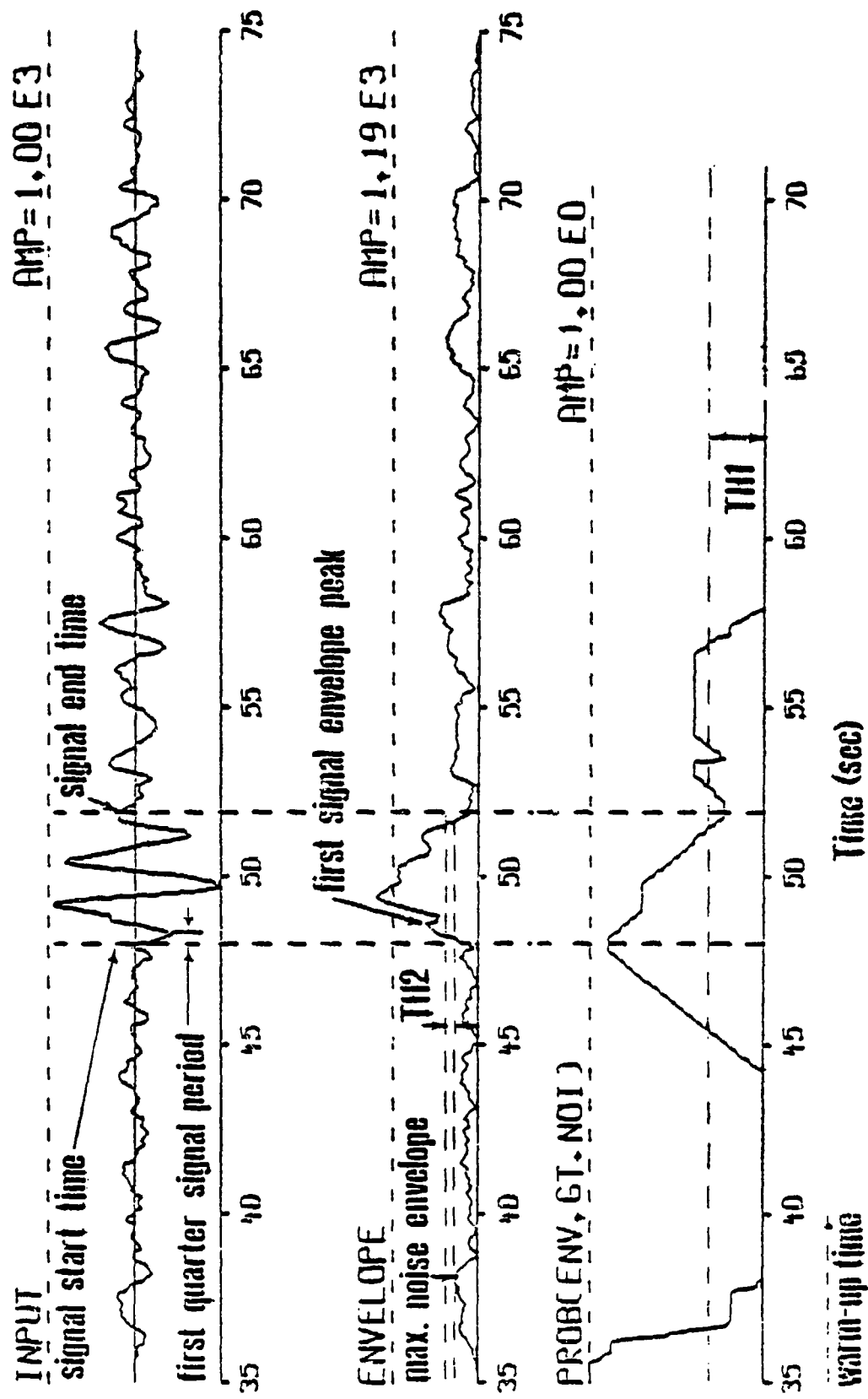


Figure 2.13. Analytic signal detection and timing (after Unger, 1978).

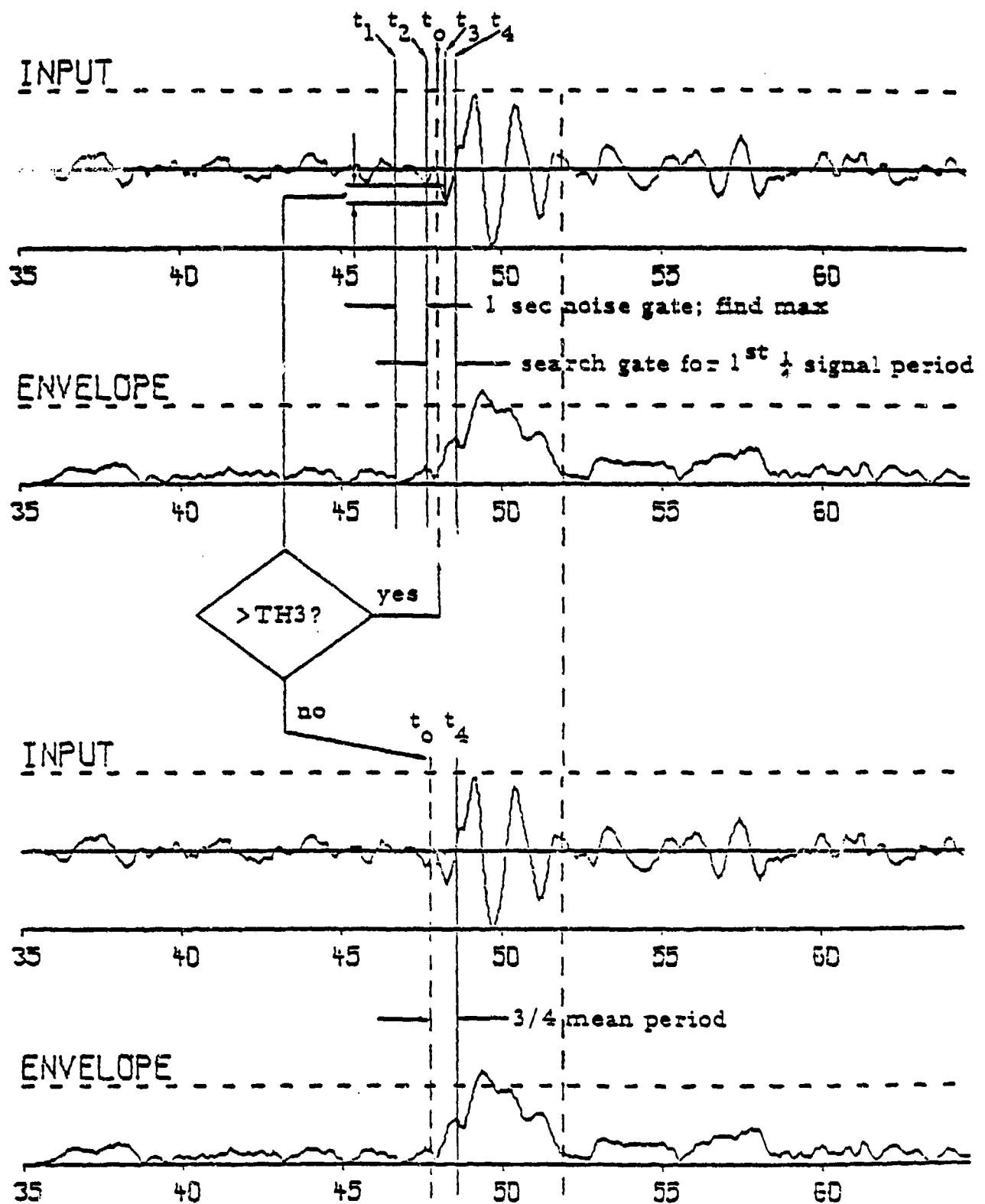


Figure 2.14. Stepback procedure in analytic signal timing (after Unger, 1978).

mean period (= 0.75/mean frequency at t_4) from the first signal envelope peak at t_4 . The mean frequency is the closed-form derivative of the phase regression polynomial evaluated at time t_4 . The search for the first quarter period is started at t_2 , i.e., at 0.8 mean period before t_4 ; the first quarter period is detected when its maximum or minimum exceeds, by a third threshold, TH3 (e.g., TH3 = 1 dB), the immediately preceding noise in the one-second time interval (t_1 , t_2).

If the second threshold (the SNR threshold) is not satisfied, the detection is annulled and the noise peak value is updated with what at first was believed to be the signal envelope peak. Thereafter, the noise peak is updated as usual, until the next supposed signal detection, etc.

The signal end time is found as the moment of the first envelope minimum occurring either after $P(|r_s(t)| > |n|_{\max})$ falls below its threshold, or after the signal duration exceeds a specified maximum, whichever is first. If this envelope minimum is greater than the tapered noise peak the noise peak envelope is updated with this value, and noise peak updating and signal detection resume as normal. This procedure enables the detection and timing of later phases and other signals in the coda."

Sax (1980) reported that, "in its present state, Unger's detector operated on a single trace at a 70 percent detection probability with about seven false alarms per hour. Its detection performance is certainly no greater, and is probably less than, that of the other detectors discussed here. Nonetheless, it has demonstrated superior performance in accurately timing P-wave signals." 

Unger (1978) tested his detector against an analyst's timing of P-wave signals. Nearly half of the events examined were timed with no apparent error. Ninety percent of the signals were timed within ± 0.5 seconds of the analyst pick. Slowly emergent earthquake signals were sometimes picked several seconds late. The standard deviation for arrival times determined using Unger's detector is 0.2 seconds. By comparison, the "Z" Detector times signals 1.70 seconds late on average, with a standard of 2.20 seconds. Thus, Unger's detector demonstrated superior capabilities for automatically timing seismic signals.

As a result of its superior capability in timing seismic P waves, Unger's detector was used in the 1979 VSC Event Identification Experiment by ENSCO to automatically time and edit P-wave signals from long seismic records. For example, a five minute record containing a possible P-wave signal is automatically processed by Unger's detector to transform it into a 50-second, signal-centered edit of the P wave.

The experience with this application was that almost all of the detected signals were accurately timed, with only a negligible number of false alarms. However, problems were encountered with missed signals. These included both impulsive signals of very short duration and gradually emergent signals. The missed-signal problem could be corrected by employing variable-length time gates for the forward-looking signal window and by using ordered noise statistics rather than the maximum noise estimates employed by Unger. In a few cases, Unger's detector inadvertently shut itself off when it encountered large glitches or spikes in the noise preceding a signal. Those cases could have been avoided by using robust median estimates of noise rather than the maximum noise estimates used by Unger.

2. Phase Detection

Unger also investigated the probability distribution for the phase $\phi(t)$. For a noise phase angle uniformly distributed between $\pm\pi$, in the absence of a signal $P(|\phi(t)| < \pi/2)$, equals 0.5. The vector diagrams in Figure 2.11 show that, when a signal is present, the phase angle is statistically biased, i.e., the above probability is greater than 0.5. For a given instantaneous SNR, this probability is:

$$P(|\phi(t)| < \pi/2) = 0.5 \quad , s(t) = 0 \quad (2.41a)$$

$$P(|\phi(t)| < \pi/2) = 1 - \pi^{-1} \arccos \frac{|\vec{s}(t)|}{|\vec{n}(t)|} , |\vec{s}(t)| \leq |\vec{n}(t)| \quad (2.41b)$$

$$P(|\phi(t)| < \pi/2) = 1 \quad , |\vec{s}(t)| > |\vec{n}(t)| . \quad (2.41c)$$

This is plotted in Figure 2.12.

For a constant SNR, this phase bias probability can be approximated by counting, within a waveform window of sufficient length, the number of times that the phase fluctuation is within $\pm \pi/2$ radians, and dividing this count by the number of window points. However, since in general the SNR will vary inside the window, this approximated phase bias probability will not relate to the SNR exactly as in Eqs. (2.44). Nevertheless, it still is some measure of the average SNR in the window, and is a good detection parameter, since it will have a value greater than 0.5 if a signal is present in the window. In this manner, phase detection is established in principle. In the application to actual data, however, there are some complications which will be discussed shortly.

The phase bias probability distribution function is compared to the envelope detection probability distribution function in Figure 2.12. We observe the important fact that the phase distribution curve reflects a detection sensitivity which is twice that of the envelope, since the arccosine argument equals the instantaneous SNR in the case of phase detection, and only one half the instantaneous SNR in the case of envelope detection. This suggests that, in principle, phase detection is at least 6 dB better than envelope detection, especially when regarding the fact that the envelope curve represents the upper bound of envelope detection sensitivity. The detection sensitivity of the instantaneous phase has been shown and used, for instance, in underwater sound propagation studies (Steinberg and Birdsall (1966); Unger and Veenkant (1967a, 1967b)." In the work of Unger (1978) this technique was applied to the detection and timing of seismic signals.

Since, in general, the signal phase varies with time in a deterministic manner (e.g., in LP dispersed waveforms), the principle of phase detection can only be applied in those cases where a model for the expected signal phase angle variations can be adequately specified. Clearly, such a model can be specified for most LP waveforms, but it is not so obvious for most SP waveforms. Also, contrary to the assumption above, the noise phase is not uniformly distributed, but may rather follow a somewhat more deterministic trend. This is the case, for instance, when the

dominant noise frequency differs from the reference frequency, f_0 , thus causing a linear phase trend. The "continuous" phase then may traverse a number of cycles within a given time gate. These facts necessitate "tracking" the instantaneous phase function; the phase fluctuations about the tracked or time-variant mean phase then may be studied for signal detection. For noise, the fluctuations should be randomly distributed; in the presence of signal they will be statistically biased. Thus, the performance of the phase detector now rests with the efficiency of the tracking process with respect to some presumed model governing the phase variations of signals, and also with the validity of the model used to estimate the signal phase angle."

Unfortunately, the rapid change of phase associated with a body wave arrival means that few sample points are available for, say, regression analysis of the phase changes, unless the data is very oversampled. This inability to track phase led Unger to abandon phase detection, the theoretically more sensitive detector, and rely simply on envelope detection.

2.5 ALLEN DETECTOR, ALLEN (1978)

This detector is based upon a heuristic detection statistic

$$E(t) = [x(t)]^2 + C \frac{dx(t)}{dt}^2 \quad (2.45)$$

where $x(t)$ is the input signal. The implementation of this proceeds as follows:

1. Calculate

$$\Delta Y_i = x_i - x_{i-1} . \quad (2.46)$$

2. Calculate

$$Y_i = \alpha Y_{i-1} + \Delta Y_i . \quad (2.47)$$

3. Calculate the "statistic"

$$E_i = Y_i^2 + C \Delta Y_i^2 . \quad (2.48)$$

We can think of the detection statistic as being formed from the weighted sum of the "power" of two filter outputs, one being a high-pass (really a bandpass) and the other a differentiator, as shown in Figure 2.15. The second filter clearly accentuates the energy near the Nyquist frequency, making good arrival time estimates possible.

The STA and LTA of the detection statistic E are calculated in the normal way with recursive filters:

$$\text{STA}_i = (1 - C_s) \text{STA}_{i-1} + C_s E_i \quad (2.49)$$

$$\text{LTA}_i = (1 - C_L) \text{LTA}_{i-1} + C_L E_i \quad (2.50)$$

Finally, an event is declared if the STA/LTA ratio exceeds some threshold value.

The rest of Allen's algorithm is concerned with verifying that the declared event is not a false alarm and with timing the arrivals. The program proceeds as follows:

1. When an event is declared the time is recorded along with Y and the first difference of Y .
2. "The program now enters a pair of nested loops in which it searches for a peak amplitude and the subsequent zero crossing. When the zero crossing is detected, the program breaks out of the loop, records the zero-crossing time relative to event onset and the signed amplitude of the preceding peak. The time and amplitude information is stored ... for later use by analysis routines" (Figure 2.16).
3. At each zero crossing of Y , the value of the STA is compared with a constant and a record kept of the number of times, S , that the STA is less than this constant.
4. The "event will be declared over when some number of zero crossings with the STA less than the constant" have occurred. This termination number, L , will be small, typically 3, at the start of an event to enable the program quickly to reject

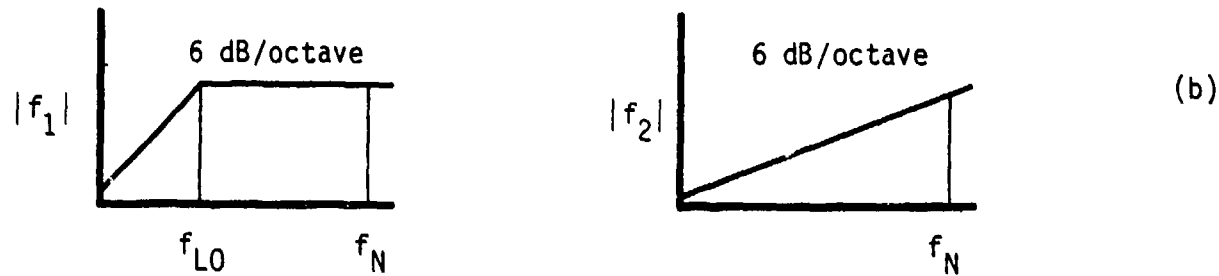
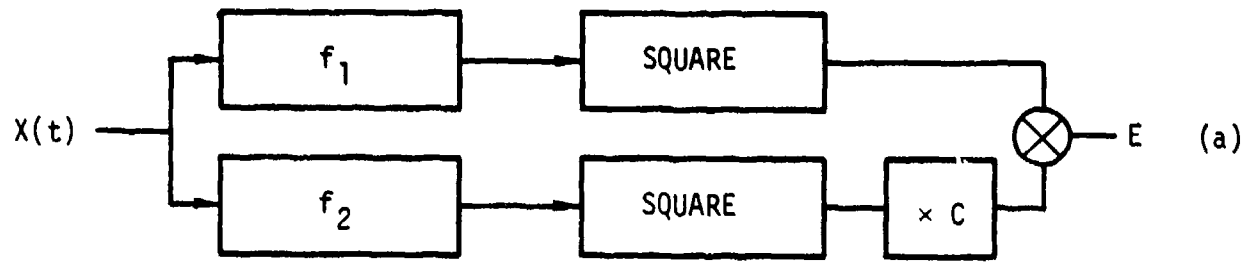


Figure 2.15. (a) Block diagram of the Allen detector and (b) the response functions of the two filter elements.

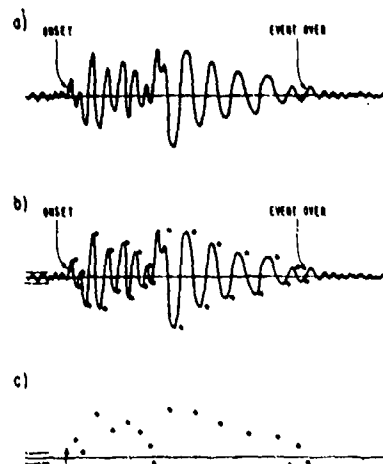


Figure 2.16. Schematic earthquake with data stored during events.
 (a) Seismic event with onset and end points. (b) Dots represent zero-crossing times and previous peak amplitudes. Amplitude bars indicate background noise preceding onset, and arrow gives first difference at onset.
 (c) Data stored for use by analysis routines after event terminates (after Allen, 1978).

noise spikes or other very short-term interference. When the algorithm is well into a larger event, however, L must be considerably larger to ensure that an earthquake observation is not terminated too early during a quiet period between phase arrivals. The present version of the program uses the relation

$$L = 3 + M/3 \quad (2.51)$$

where M is the current number of observed peaks in an event.

5. This decision of whether the event is over is simply a comparison of S and L, with branches to continue the program in the observation loop or to terminate observation of the event as required."
6. A test is made for the duration of the event to eliminate such noise bursts as line spikes, etc. For small local events, Allen used typically the criterion that the event should be longer than 1.5 seconds and have recorded more than 40 peaks.

The performance statistics currently available on Allen's detector are based on local seismic network data sampled 200 times a second. The results obtained are extrapolated below to those for a 20-Hz-sampled regional or teleseismic network.

The operating characteristics demonstrated by local network operation show a 70 percent detection of analysts' picks, with 36 false alarms over 44 hours of operation. Allen's detector also grades the quality of signal detections. None of the 36 false alarms was graded at the highest level of reliable detections.

Allen's detector times local event signals to a standard deviation of 0.05 seconds with 200-Hz local network data. This would scale to 0.5 seconds for our 20-Hz data, much better than the 2.2 second standard deviation of the "Z" Detector.

In comparison with the "Z" Detector at the level of 70 percent detection probability, the Allen Detector operated with 0.82 false alarms per hour as a local event detector compared with 0.4 false alarms per hour of DET 459 and with 0.8 false alarms per hour at KSRS. By design, the "Z" Detector is expected to maintain a more stable level of false alarm control. Allen's detector concept applied to the detection of regional and tele-seismic signals sampled at 20 Hz is now being studied by ENSCO's DSC Division.

It is interesting that Allen's detector operates on a completely different principal than does the "Z" Detector. The power of Allen's detector stems from the sophisticated post-detection analysis of possible signals which is designed to eliminate most false alarms. The frequency is estimated by counting zero crossings. Also, the time duration of the signal is estimated. A minimum event duration of 1.5 seconds and an acceptable range of frequencies are some post-detection analysis requirements for accepting detections as representing valid signals.

There appears to be room for a substantial performance gain in detecting P waves by using the Allen Detector, and especially by optimizing the post-detection analysis for that purpose. The detector requires a limited memory (about 1.0 K bytes) and a very modest computer capability. The characteristic function and post-detection processing of the Allen Detector is in a form most suitable for optimizing and training the automatic detector to track the performance of experienced analysts.

2.6 THE STEWART DETECTOR, STEWART (1977)

This detector uses an algorithm that was designed to mimic the mental process that a trained analyst performed on a seismic trace. A nonlinear high pass filter is applied to the signal to transform it in such a manner that:

- a. The oscillatory nature of the signal is preserved;
- b. The direction of the first motion is preserved;
- c. It high passes the signal in the normal manner, thus reducing the D.C. and drift components;
- d. Slightly emergent onsets of seismic signals are enhanced.

The transformation process is illustrated in Figures 2.17 and 2.18. The "algorithm computes the modified seismic signal MDX_k from the incoming signal X_k , where k represents the current time epoch. The results of applying this transformation to a 1-Hz and a 3-Hz sinusoidal signal are shown in Figure 2.18. From this figure the high-pass nature of the transformation is apparent.

The first step in the transformation process (Figure 2.17) is to compute the simple first difference of the incoming signal ($DX_k = X_k - X_{k-1}$ where k represents the current time epoch). The sign of the current first difference DX_k is compared to the sign of the previous first difference DX_{k-1} . If the signs are the same, and if this sign has persisted for less than eight consecutive times, then the value of the modified signal MDX_k is taken to be its current value increased by DX_k . Otherwise, the value of the modified signal is taken to be DX_k . This technique transforms the incoming signal in such a way that the four objectives listed above are accomplished. "This modified seismic wave form is the basis for nearly all signal analysis by the on-line system.

The one exception to this is that the maximum signal amplitude is determined from the incoming seismic signal X_k .

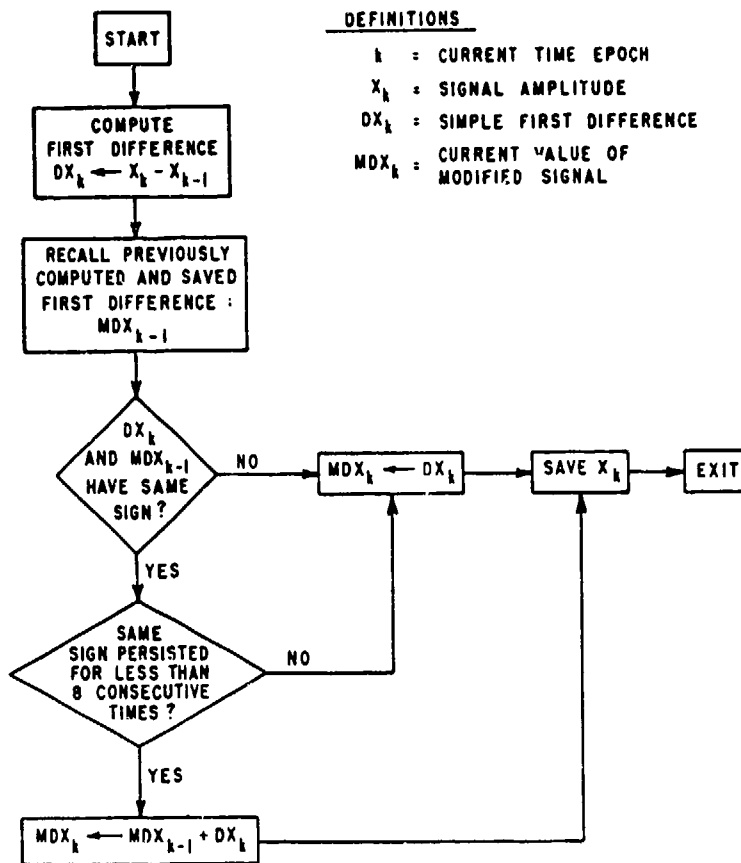


Figure 2.17. Processing steps to compute the modified seismic signal MDX_k from the incoming signal X_k . The modified signal is used extensively in the detection logic of the on-line system (after Stewart, 1977).

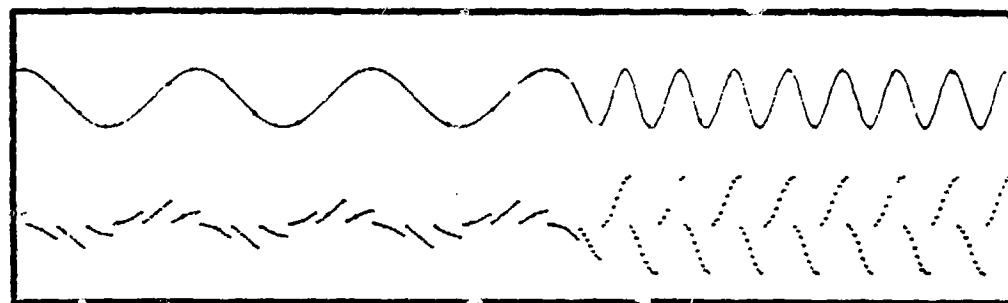


Figure 2.18. Effect of the filtering operation (summarized in Figure 2.17) on a 1 Hz and 3 Hz sinusoidal signal. The upper signal is the unfiltered analog output of a function generator, fed simultaneously to one channel of the on-line system and to a chart recorder. The lower signal is the filtered function MDX_k computed in real-time by the on-line system and routed through a digital-to-analog converter to the chart recorder. Digitizing rate is 50 samples/second. Peak amplitude of the 3 Hz filtered signal is approximately twice that of the 1 Hz signal (after Stewart, 1977).

The long-term averages of three quantities are computed;

1. The mean of the signal itself

$$LTA1_i = (1 - C1) LTA1_{i-1} + C1 X_i .$$

2. An estimate of the standard deviation of the signal is made by calculating the LTA of the absolute value of the variations of the signal about its mean

$$LTA2_i = (1 - C2) LTA2_{i-1} + C2 |X_i - LTA1_i| .$$

3. A similar estimate of the standard deviation of the modified signal is the LTA of the absolute value of the MDX_i

$$LTA3_i = (1 - C3) LTA3_{i-1} + C3 |MDX_i|$$

where $C1$, $C2$ and $C3$ are the filter constants.

These quantities are intended to characterize the signal under the no-event hypothesis and thus updating their values is suspended if a tentative event is detected. The detection algorithm is a two-stage process with the first stage detection test being simply a test of whether $MDX_i/LTA3_i$ is larger than some constant $C4$.

When a tentative detection is made, the algorithm proceeds to the post-detection stage designed to reduce the FAR. Stewart (1977) divides this process into two modes, the P-phase processing and the coda processing.

The P-phase processing continues for 0.5 second after the tentative detection is declared. (The data he considered were sampled at 50 sps.) During this interval, the following four criteria must be met to proceed or else the tentative detection is cancelled:

$$1. \left| \frac{MDX_i}{LTA3_i} \right| > C4 \quad N1 \text{ times};$$

2. The time duration for which

$$\left| \frac{MDX_i}{LTA3_i} \right| < C4$$

must not exceed 0.28 seconds consecutively;

3. $|\max X_i| > C5$

4. $\left| \frac{\max X_i}{LTA2_i} \right| > 8 .$

If these four tests are passed, the algorithm then proceeds with the coda processing. This process continues for a time interval determined by testing

$$\left| \frac{MDX_i}{LTA3_i} \right| > C6 ,$$

if this test fails for a continuous 2 seconds, the coda processing is terminated. The following three tests must be passed during this phase of the algorithm.

1. Coda length must be ≥ 4 seconds;

2. $\left| \frac{MDX_i}{LTA3_i} \right| > C6$ and $\left| \frac{MDX_j}{LTA3_j} \right| < - C6$

is alternating sequence at least six times;

3. The number of oscillations of MDX_i must exceed $0.5 H_z/time$ duration of coda.

This algorithm was implemented by the USGS using data from their central California and Oroville networks. Stewart (1977) reports on test results from this network obtained during a one month period which included a large aftershock sequence near Oroville.

Table 2.1 (after Stewart, 1977) summarizes the results of both detection and on line location for the Oroville network while Table 2.2 (also from Stewart, 1977) summarizes the results for one month of operation on the central California network.

TABLE 2.1
DETECTION AND LOCATION CAPABILITY OF REAL-TIME SYSTEM FOR THE
OROVILLE SEISMIC NETWORK DURING OCTOBER 1975

<u>No. of Events</u>	<u>Percentage</u>	<u>Comment</u>
107	90.7	Detected and located.
8	6.8	Detected but not located, because data were too noisy or too sparse.
1	0.8	Not detected.
2	1.7	Not detected, preceded within 60 seconds by another event
<hr/> 118	<hr/> 100.0	

TABLE 2.2

DETECTION CAPABILITY OF REAL TIME SYSTEM FOR THE CENTRAL
CALIFORNIA SEISMIC NETWORK DURING OCTOBER 1975

<u>No. of Events</u>	<u>Percentage</u>	
225	86.5	Detected.
25	9.6	Not detected, events north of 38°30'.
5	1.9	Not detected.
3	1.2	Not detected, computer maintenance in progress.
2	0.8	Not detected, preceded within 60 seconds by another event.
<hr/>	<hr/>	
260	100.0	

A portable field recorder, Teledyne Geotech's Model MCR-300 Microcorder (Veith, 1978), which uses this algorithm, has been developed and tested. The tests were run on two field units operating at the Nevada Test Site where the noise sources, both natural and cultural, varied both in character and time. Data was sampled at rates varying from 20 sps to 200 sps for several days. Comparison between the results of this algorithm and the "standard STA/LTA" algorithm was made. The main results of these tests were:

1. "Once triggered, the STA/LTA detector often shut down during a relatively low signal period only to trigger again after a second or two. The algorithm detector did not shut down until the end of the signal.
2. An "emersio" signal would not trigger the algorithm unless it contained a higher amplitude energy burst. The STA/LTA detector often triggered from "emersio" signals. (Emersio is used here in the sense that both the long and the short term averages are increasing slowly in the STA/LTA ratio is near the specified SN value.)"

Veith (1978) finally concludes that, "tests on limited data show the algorithm can ignore noise while detecting earthquake energy. It can make the transition between changes in noise level with every little difficulty and record seismic signals within virtually any background without changing the settings of the algorithm parameters. The algorithm will record complex signals without the termination problems typical of the STA/LTA detector.

While the tests gave very good results in detecting seismic events, they were not perfect. It may be possible to develop additional simple tests during the field test period which would provide a more powerful discriminant. The principle difficulty lies in obtaining tests which may be passed by microearthquake signals, teleseisms or surface waves in accordance with the pass band selected."

2.7 WALSH DETECTOR, GOFORTH, T. AND E. HERRIN (1980)

This detector is based on the representation of the digital seismic signal **in terms of Walsh functions**. These form an ordered set of rectangular waveforms which are either +1 or -1. They are ordered according to the number of zero crossings per interval. Like the exponential functions of the Fourier transform, they form an orthonormal set over some interval. Thus, the sampled seismic signal x_j can be represented in terms of its Walsh transform coefficients by,

$$x_j = \sum_{k=0}^{N-1} w_k \text{Wal}(k,j) \quad (2.52)$$

where

$$w_k = \frac{1}{N} \sum_{j=0}^{N-1} x_j \text{Wal}(k,j) \quad (2.53)$$

and k is termed the sequency. Figure 2.19 illustrates the Walsh functions $\text{Wal}(N,i)$ for $N = 0, \dots, 8$. This transformation may be compared to the discrete Fourier transform pair of:

$$x_j = \frac{1}{N} \sum_{k=0}^{N-1} F_k e^{i\omega k j} \quad (2.54)$$

where

$$F_k = \sum_{j=0}^{N-1} x_j e^{-i\omega j k} \quad (2.55)$$

and

$$\omega = \frac{2\pi}{N} \quad (2.56)$$

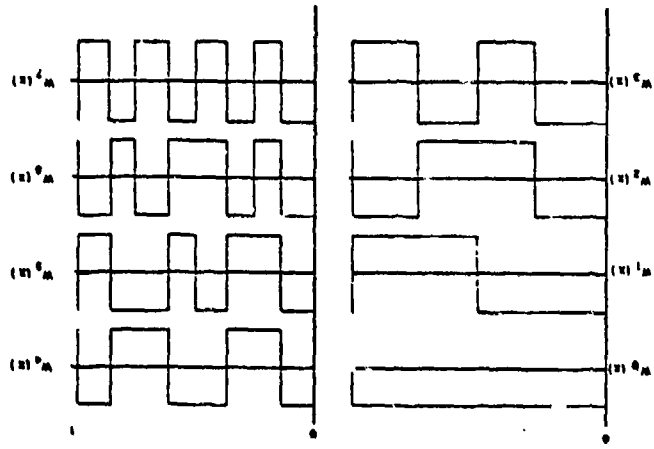


Figure 2.19. The first eight Walsh functions.

Obviously, since Walsh transforms are generated using simple rectangular + or - unity functions rather than sines and cosines, they may be calculated much more efficiently (quicker) in a computer. Clearly, to generate the Walsh transform of the discrete x_j , all that must be done are logical compares and adds. Performing functions such as prewhitening and filtering will similarly be much more efficient than their time domain or Fourier transform counterparts. Indeed, the purpose of this detector is speed or computational efficiency in the implementation of concepts used in other detectors.

A block diagram of the detection algorithms is shown in Figure 2.20. The digital data is analyzed in 64 sample windows (3.2 seconds for 20 sps data) with a 32 sample overlap. The analysis proceeds as follows:

1. The Walsh transform of the 64 data samples is calculated

$$W_k(x) = \frac{1}{64} \sum_{j=0}^{63} x_j \text{Wal}(k,j) \quad k = 0, \dots, 63 \quad (2.57)$$

2. The Walsh coefficients are multiplied by prewhitening weights N_R calculated beforehand (see below).
3. Weights B_k of 0 or 1 are applied to isolate the fixed signal band.
4. The absolute values of the weighted Walsh coefficients are summed to give the final detection "statistic"

$$Y = \sum_{k=k_1}^{k_2} |W_k \cdot N_k \cdot B_k| \quad B_k = 1 \quad k_1 \leq k \leq k_2 \quad (2.58)$$

$$= 0 \text{ for other } k \quad (2.58)$$

The detection statistic Y is thus equivalent to the STA here calculated over at 3.2 second gate for 20 sps data.

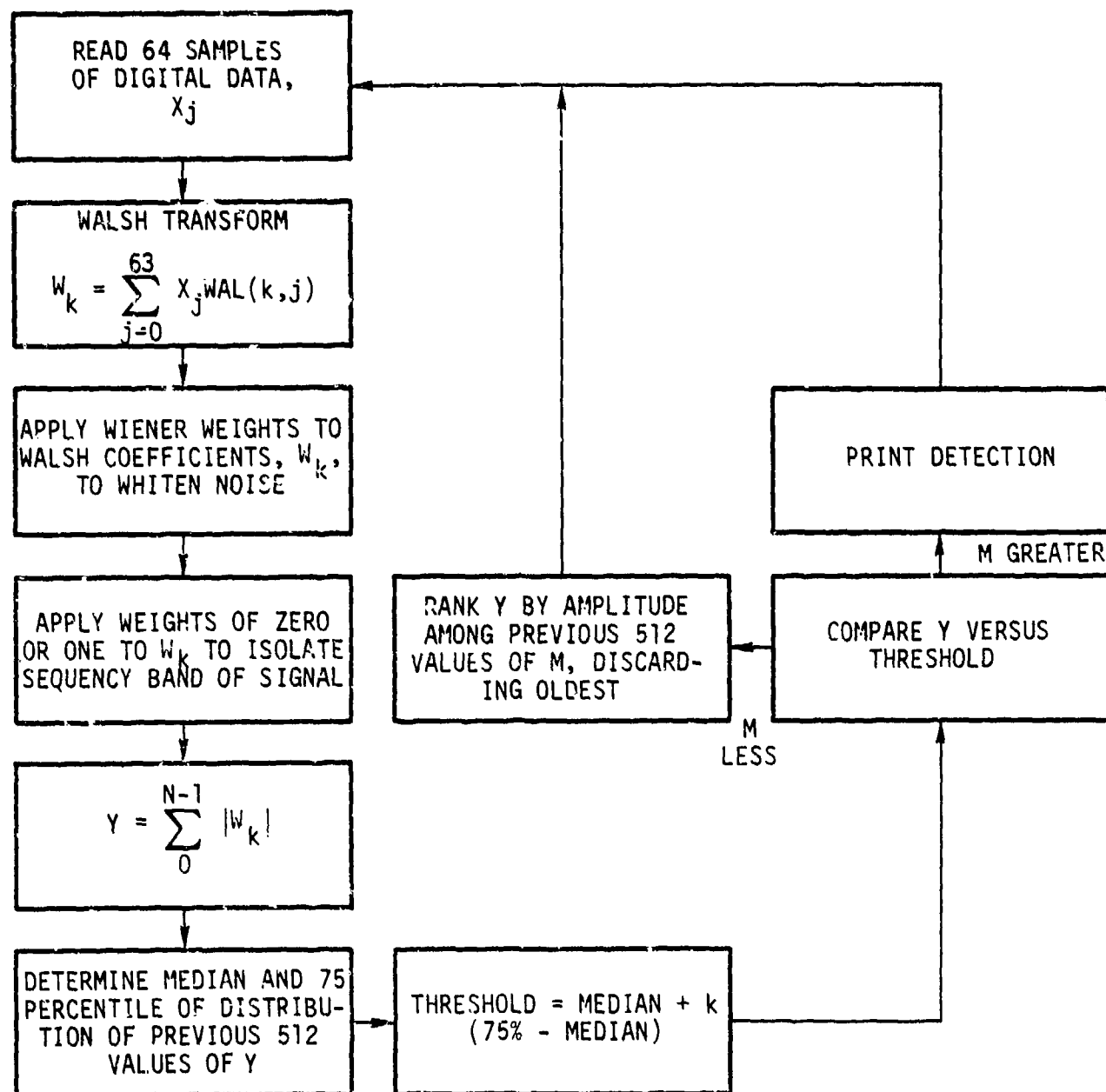


Figure 2.20. Walsh detector flow diagram (after Goforth and Herrin, 1980).

The prewhitening weights N_k are currently calculated in a non-adaptive manner as follows:

1. A 34 minute sample of noise is selected.
2. The Walsh transform of 640 consecutive 64 sample windows is calculated.
3. The mean of the absolute values of each of the 64 Walsh coefficients is computed.
4. Weights of the form $2 \cdot n$, where n is an integer, are selected to whiten the means in each subsequence band.

The detection threshold against which the statistic Y is tested is calculated from the median value Y_{50} , and the 75 percentile value Y_{75} of the previous 512 values of the STA (14 minutes) by the weighted combination.

$$\text{Threshold} = (1 - k) Y_{50} + k Y_{75} . \quad (2.59)$$

The coefficient, k , is typically five. Note that this is not the same as the action of a recursive filter on Y . If Y is Gaussian distributed with mean μ_Y and variance σ_Y^2 then

$$Y_{50} = \mu_Y$$

$$Y_{75} = 1.5 \sigma_Y .$$

Thus, in this case,

$$\text{Threshold} = \mu_Y + 5 (1.15 \sigma_Y - \mu_Y) . \quad (2.60)$$

If the current value of the sum of the absolute values of the Walsh coefficients exceeds the threshold for two consecutive time windows, an event is declared. If it does not exceed the threshold, the sum of the absolute values, Y , is ranked among the previous 512 values, the oldest value being discarded. In this way an adaptive detection threshold

is maintained, the adaptation window being approximately 14 minutes. If a signal is called, the threshold is not updated.

Three separate tests of the Walsh detector have been reported by Goforth and Herrin (1980). Two consisted of tests conducted on simulated data constructed of noise plus scaled 8 second long segments of a Novaya Zemlya explosion added at specific times to the noise samples. The noise samples were taken from:

1. The SMU KS36000 seismometer at Dallas with the signals added at a SNR of 1.0 and 0.75.
2. The ANMO SRQ with the signals added to scale a 4.5 m_b and 4.2 m_b event.

The results of these tests were:

- 1a. 80 detections (100%) 0 false alarms
- b. 40 detections (100%) 1 false alarm
- 2a. 39 detections (97.5%) 0 false alarms
- b. 36 detections (90%) 1 false alarm

Finally, the detection algorithm was run on the center element of one of the NORSAR subarrays for a five hour period of data. The results were a seven out of eight detection success (missing a 3.6 m_b at 6,222 km epicentral distance) with a FAR of 0.6/hour. In another overlapping seven hour test, the algorithm succeeded in detecting nine out of ten events (including a local teleseism that the NORSAR beams missed) with a FAR of 0.86.

2.8 MARS DETECTOR, MASSO, et al. (1979)

The MARS (Multiple Arrival Recognition System) detector uses quasi-harmonic decomposition to analyze a broadband signal by passing it through many narrow band filters. One thus obtains a time-frequency breakdown of the non-stationary signal power. An "event" consists of a statistically significant fluctuation from the random background pattern of the instantaneous spectrum. There are certain strong affinities between the MARS detector and the deflection detector described in Section 2.3, particularly the "average deflection" (3) version. Both use frequency domain methods, and both search for short term increases in power over an adaptive frequency band. Unlike the deflection detector, however, the MARS detector does not calculate directly a statistic, but rather contains a highly nonlinear and adaptive pattern recognition algorithm which seeks undispersed alignments of peaks in the narrow band envelope functions. The function of the STA, the fundamental time T_0 , is roughly dependent on the Q of the filters, for the narrower the frequency resolution, the larger the time duration of the impulse response. There is also inherent in the method an LTA, for envelope maxima only have meaning to the extent they deviate from past behavior. But even though these two concepts carry through in the MARS detector, they do not appear in a mathematically tractible form, since the final decision is based principally on a band width and dispersion criterion.

The concept of a detector based upon multiple band pass filters goes back at least to Moltshan, et al. (1964), who stated:

"The signal from the seismogram is passed through a group of linear filters. All filters are divided into several, in our case, two, sub-groups. In each sub-group the filters have the same pass band, but difference resonance frequencies; their pass bands are not overlapping and cover the whole range of frequencies. Then the output of each filter is compared with some threshold which is chosen according to the level of noise in this filter. If in at least one of the filters the threshold is surpassed, then the presence of a useful signal -- the alarm -- is announced. The record may begin slightly before the alarm; which is why a delay line is desirable."

The potential advantages in this technique lie in the area of adaptability and in signal characterization. This latter aspect, indeed, was powerfully utilized in the work of Masso, et al. (1979) which involved both detection and discrimination of seismic signals. They describe the detection part of the MARS processor as follows:

"The central feature of the detector module is the use of a set of narrow-band frequency filters to break up or decompose a time series consisting of signal plus noise into a set of quasi-harmonic modulated "signals." This set of filtered signals, one for each filter of center frequency f_c , can then be used to determine the energy arrival time (or group arrival time, t_g) and amplitude of the original broad-band signal by analysis of the time modulation of the filter outputs. Further, both the instantaneous phase and frequency of the individual filter outputs, that is the apparent phase and frequency of the quasi-harmonic filter outputs as a function of time, can be determined quite simply. Thus, the decomposition of the original signal wavetrain, possibly composed of many individual signal pulses, into quasi-harmonic signals provides the means of determining arrival time, amplitude and phase, all as functions of frequency. This then is the basic signal information that can be used to detect a given type of signal in terms of its dispersion characteristics and to obtain its spectrum as well as its time and amplitude relationship with respect to other signals present in a complex wavetrain.

The basic approach is to identify patterns from the signal and noise information as it is expressed in the $t_g - f$ plane (the group arrival time, t_g , versus frequency plane). The pattern to be searched for in the $t_g - f$ plane will correspond, in the case of a body wave, to a (nearly) undispersed signal, with spectral amplitude significantly above background in a frequency range corresponding to some fraction of the total band. This frequency band will be in a range where the signal power is expected to be highest relative to noise. (This means we will make use of the matched filtering concept, in the sense that we know roughly what spectral content we expect for the signal. This concept is also used when we look for only undispersed signals or signals of known dispersion characteristic.) Thus, in the $t_g - f$ plane one would search

for a straight, horizontal line-up of envelope maxima in a selected frequency band, using the largest maxima as the beginning point in such a pattern recognition procedure. This, therefore, implicitly, uses a threshold detection criteria in a detection band, since by starting with the largest envelope maxima we are essentially requiring that the signal power be above the background level in at least a part of the detection band.

Basically, then, by looking in this $t_g - f - A_g - \phi_g$ space, we will apply criteria based on properties of the expected signal, namely its expected dispersion and spectral content, in order to recognize a signal pattern and to thereby detect the signal. An example of how this is accomplished is shown in Figure 2.21. In this figure we plot the times (t_g) of the envelope maxima from narrow band filter outputs, with of the order of $N = 20$ filters used so that the signal frequency content is sampled at about 20 points, f_n . With each envelope maxima point in the plane, there is also an associated (spectral) amplitude $A_g(f_n)$, instantaneous phase $\phi_g(f_n)$ and an instantaneous frequency $(d\phi/dt)_{t_g}$. Thus, the $t_g - f$ plot corresponds to a multidimensional display of spectral content and energy arrival time for a given segment of a time series. Normally either 1,024 or 2,048 points are used for time segments, and for short period seismic data this corresponds to a 50 to 100 second segment which is processed in each pass. For on-line continuous processing, overlapping time segments will be used.

A sub-band within the entire frequency range covered by the set of filters is shown in Figure 2.21 and is used as a "detection band," that is, a frequency band within which a signal pattern (straight horizontal line locus of envelope maxima in the case of an undispersed body wave) is sought. This band, from f_L^* to f_H^* , is selected externally, based on the expected signal frequency character. The largest envelope maxima within this band are flagged (denoted by \boxed{X} in the figure) and used to compute a mean "signal" arrival time (i.e., group time) \bar{t}_g for the maximum power arriving in this frequency range. An acceptance window in time, for which maxima can actually be associated with an undispersed signal, can be constructed using the relation: $\bar{t}_g \pm t_\sigma^\pm \pm \alpha \Delta t$; where Δt is the time uncertainty associated with the envelope maximum

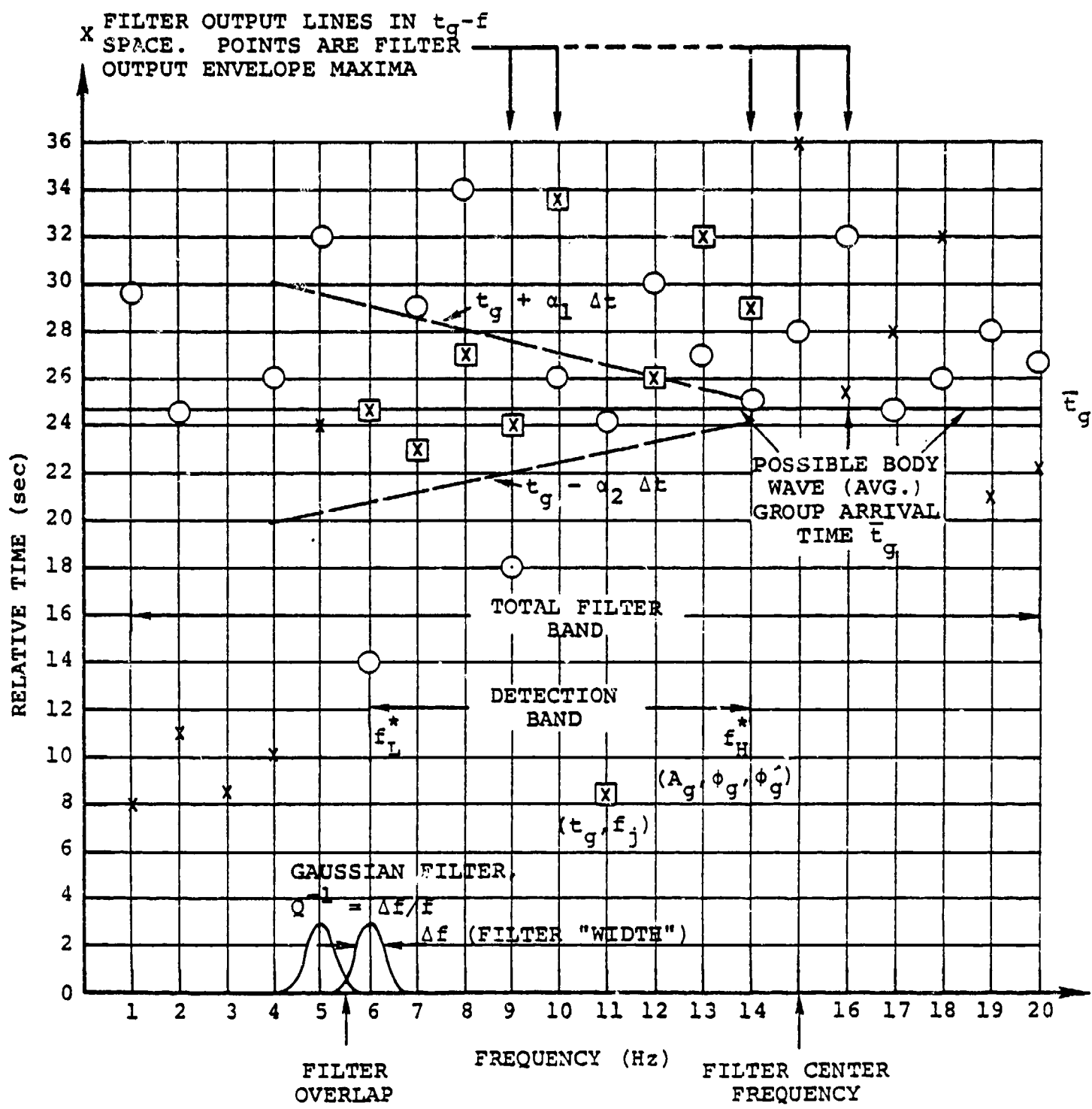


Figure 2.21. Typical t_g -f plane representation of a time series segment (0 to 36 sec) when the signal-to-noise ratio is low. Only the largest envelope maxima (X) and second largest maxima (O) are shown. Other, numerous, smaller envelope maxima are normally scattered throughout the t_g -f plane, but for this illustration they have been omitted. Each filter "output line" normally displays about ten such peaks.

time t_g for a filter output at center frequency f and half power band width Δf . In particular, $\Delta t \Delta f \geq 1/4\pi$ is the theoretical uncertainty relation and since $\Delta f/f = Q^{-1}$, then $\Delta t \geq 1/4\pi (Q/f)$. Further, we use t_σ to denote the standard deviation in the time data used to compute t_g and make use of it to define the acceptance time window about \bar{t}_g as well. Hence, taking an appropriately chosen constant α near unity, then two time window boundary lines can be defined to give the time window; that is: $\bar{t}_g + t_\sigma^+ + (\alpha/4\pi)(Q/f)$ and $\bar{t}_g - t_\sigma^- - (\alpha/4\pi)(Q/f)$. All of the largest maxima within such a window are then to be taken as acceptable undispersed "signal" group arrivals. Those outside would be rejected and the second largest maxima could then be tried, and so on. If the number of peaks accepted in the window is lower than some specified lower limit, then the tentative "signal" detection would be rejected and reclassified as noise."

As currently implemented for the SDAC detection experiment, the algorithm can be described by the flow diagram given in Figure 2.22. A difference between MARS and most other detectors appears right at the beginning, in that quite long (say 100 seconds) signal windows are typically used.

Fourier transform methods are used to derive 20 or so narrow band envelope functions. A heterodyne operation applied to the windowed frequency function means that the algorithm effectively calculates one forward and two (rather than 20) inverse transforms.

With the 100 second sample of envelope function available, the MARS detector quickly zeros in one the most likely candidate "event" by searching for the largest envelope maximum in each band, and averaging their occurrence times. A generous search window is constructed about this averaged time, within which undispersed alignments of envelope maxima are sought. It is at this stage that a threshold amplitude value, based upon the LTA for each frequency band, is used to sort out only the "large" peaks. After this stage, the actual value of an envelope maximum is never used. If a significant number of frequency bands show well aligned envelope peaks (or energy arrivals), an event is called and its arrival time within the window noted. Otherwise, the LTA, or

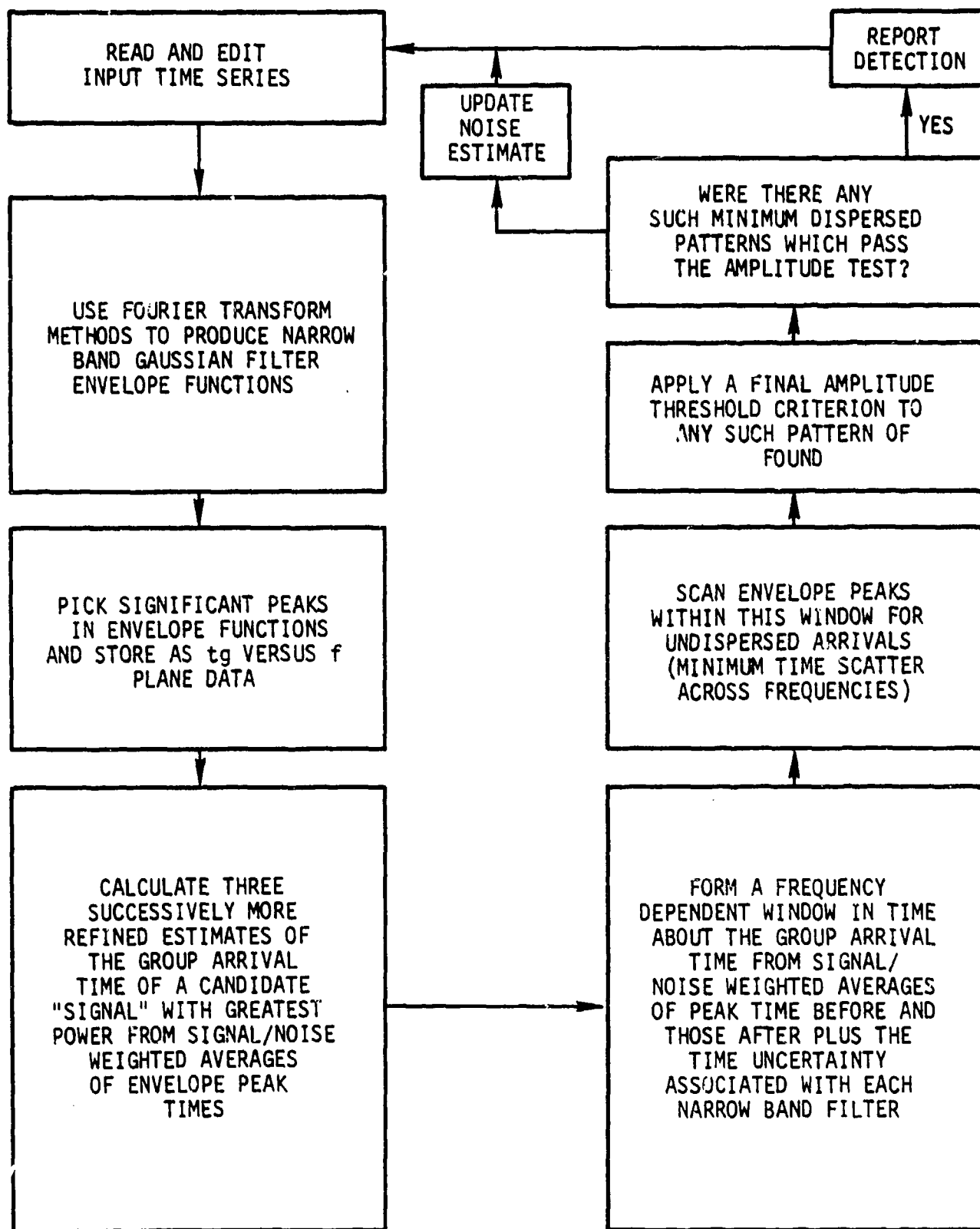


Figure 2.22. MARS detector flow diagram.

noise threshold, in each band is updated and the next block of data processed.

Although a key part of the MARS analysis in the SDAC discrimination experiment was reliable performance of the detector algorithm, the dependence of FAR on program variables has only been studied in the past six months. These noise studies, as well as processing of the SDAC detection test tape have yielded quantitative values for the receiver operating characteristic.

In the recent report by Farrell et al. (1980), it was concluded that "The MARS seismic event detector offers a significant improvement over the current VSC optimally-filtered STA/LTA detector. On nearly 45 hours of synthetic data, MARS detected 13 percent more events than the STA/LTA detector, demonstrating its capability of extracting low-level signals in a poor SNR environment. The additional events detected by MARS are nearly all small amplitude...events. The advantage of the MARS algorithm at low signal levels should not be surprising since MARS is not simply a power-law detector but also uses the signal dispersion and bandwidth as discriminating characteristics.

The improvement in detections was achieved with no attendant increase in the false alarm rate. In fact, with the NORSAR data, the MARS FAR was only two-thirds that of the STA/LTA detector. The MARS FAR with the Pinedale data is equal to that of the STA/LTA detector. It is likely that the MARS FAR can be lowered with the implementation of more discriminating detection tests, but the present level of MARS detections is close to the theoretical limit predicted for an ideal matched filter and is unlikely to be greatly increased by any means.

The ten percent advantage in probability of detection shown by the MARS detector for this particular class of events is equivalent to an improvement of about 0.1 in body wave magnitude. This is, the MARS detector should have nearly the same probability of detection and same false alarm rate as the benchmark VSC detector, but for signals which are an average of 0.1 magnitude smaller."

III. CONCLUSIONS AND RECOMMENDATIONS

1. All detectors reviewed in this report are based on a comparison between some form of variance estimate of the signal calculated over a time period approximately equal to the duration of an expected seismic "event," and the normal (or long term) variance.

Possible exceptions to this general form are the phase detector described by Unger (1978) and the similar part of MARS. The former did not work because the short period phase fluctuations were so rapid that they could not reliably be predicted; the latter has not been implemented.

2. Ad hoc detection algorithms such as Allen's and Stewart's (1977) offer a hope of some improvement in the ROC of the detection process. These methods, after having made the basic detection statistic test and having made a tentative identification, are followed by a further process that is designed to:
 - a. reduce the false alarm rate,
 - b. improve the timing capability, and
 - c. speed the recovery of the detection algorithm after an event is encountered.

How much these algorithms can be expected to offer significant improvements in the ROC depend upon where on these curves they are operating. If the SNR is such that a high probability of detection is achieved with a tolerable FAR, then little improvement can be expected. If, however, the SNR is poor so that the probability of detection is low for a given FAR, then significant improvement may be achieved by such two-stage algorithms.

3. Testing of the detectors described in this report was not carried out in a uniform manner on the same or even similar data sets. Thus, no definitive statement about their relative

performance may be made. However, it appears that no one detector is obviously superior to all others. Some have been optimized for teleseismic detection using a moderately large computing facility. Some have been designed for operation in microprocessor controlled field recording units, typically used in the near field or at least at regional distances. These applications stress ease of implementation in microprocessors. Some algorithms stress detection timing accuracy as this may be another object of the algorithm.

4. Little theoretical advance has been achieved since Frieberger's 1963 work in which he "solved" the problem of detection of a Gaussian signal in Gaussian noise. The influence of this work has rightly guided the design and implementation of many of the detectors used today. However, it must not be thought that the "real problem" has been solved. The "real problem" is the detection of certain non-Gaussian signals in the presence of non-Gaussian noise. Frieberger discovered the optimum detector for an approximate model of the actual situation, but other algorithms may work significantly better on "real" data. Further, considerations such as timing ability, recovery of the algorithm after an event, and immunity to highly non-Gaussian noise such as line spikes and data drop outs may dictate very different approaches.

RECOMMENDATIONS

- Uniform testing of all viable detectors should be conducted with
 - a. a realistic synthetic data set,
 - b. all detectors coded for and running on the same or similar machines; and
 - c. ROC curves produced for each detector.
- Theoretical and experimental research in phase sensitive detectors should be supported as this is an area where it may

be possible to exploit signal information not used in energy or power detectors.

- Research should be encouraged to test if matched filters for specific types of signals (station/source pairs) improves detector performance.
- Further development of hybrid detection algorithms, that combine high probability of detection with a high FAR and then are followed by a post processing to reduce the FAR should be undertaken.
- New algorithms, designed specifically for use with the new generation of three component broad band seismographs, should be developed and tested.
- In view of data rates from these new data sources, dedicated microprocessors to run the detection algorithms on a one processor per channel (or seismic station) basis should be considered.

IV. ACKNOWLEDGMENTS

The authors would like to express their appreciation to Dr. Robert Blandford for his help in preparing this report and to Dr. W. E. Farrell who was largely responsible for Section 2.8 and who contributed significantly to the entire report with his critical review and constructive suggestions for improvement.

V. ABSTRACTS OF PRINCIPAL PAPERS

Allen, R. V. (1978), "Automatic Earthquake Recognition and Timing from Single Traces," BSSA, 68, pp. 1521-1532.

Abstract: A computer program has been developed for the automatic detection and timing of earthquakes on a single seismic trace. The program operates on line and is sufficiently simple that it is expected to work in inexpensive low-power microprocessors in field applications. In tests with analog tapes of earthquakes, the program correctly identified and timed to within 0.05 sec about 70 percent of the events which would normally be timed in operation of a network. The program evaluates the accuracy of its picks, and its estimates appear to be quite reliable. The algorithm is working at present in a 16-bit minicomputer and appears to be compatible with presently available microprocessors.

Farnbach, J. S. (1975), "The Complex Envelope in Seismic Signal Analysis," BSSA, 65, pp. 951-962.

Abstract: Some practical implications of the complex envelope representation of seismic signals are presented. Beginning with a look at an artificially constructed signal and proceeding to seismic records, it is seen that the complex envelope is more amenable to visual interpretation than the real signal itself. This is attributed to the natural separation of amplitude information from angle information afforded by the complex representation, and examples of arrival time measurement and P-coda correlation suggest that this leads to concrete seismological benefits. On this basis, it is suggested that the complex envelope may be a useful tool in seismic signal analysis.

Frieberger, W. F. (1963), "An Approximate Method in Signal Detection," Quarterly Appl. Math., 20, pp. 373-378.

Abstract: A theorem from the theory of Toeplitz forms is applied to the problem of estimating the best test statistic for the detection of Gaussian signals in Gaussian noise.

Goforth, T. and E. Herrin (1980), "Semiannual Technical Report," Air Force Office of Scientific Research, Contract No. F49620-76-C-0030, Dallas Geophysical Laboratory, Southern Methodist University.

Abstract: An automatic seismic signal detection algorithm based on the Walsh transform has been developed. Since the amplitude of a Walsh function is either +1 or -1, the Walsh transform can be accomplished in a computer with a series of shifts and fixed point additions. The savings in computation time makes it possible to compute the Walsh transform and to perform band-pass, pre-whitening and adaptive filtering with a micro-computer in real time for use in signal detection.

The algorithm has been programed in FORTRAN on a Raytheon Data Systems 500 mini-computer. Tests utilizing seismic data recorded in Dallas, Albuquerque, and Norway indicate that the algorithm has a detection capability comparable to a human analyst. The Walsh detection algorithm runs in approximately 1/10 real time on the RDS-500 mini-computer. Programming of the detection system in machine language on a North Star Horizon microprocessor-based computer is almost complete. Run time on the Horizon is estimated to be 1/3 real time.

Shensa, M. J. (1977), "The Deflection Detector, Its Theory and Evaluation on Short-Period Seismic Data," Report TR-77-03, Texas Instruments, Alexandria, VA.

Abstract: This study investigates the application of a deflection detector to short-period seismic data. In general, for power detectors, no single filter will be optimal for a large variety of signals in a dynamic noise environment. The deflection detector represents an attempt to adapt to such a situation by utilizing individual FFT frequency cells as a bank of filters which can accommodate a broad variety of signals. The performance of the deflection detector is analyzed and compared to that of the power detector for several seismic signals. It is concluded that the deflection detector shows a distinct advantage when the variety of signal spectra to be detected is sufficiently large.

Stewart, S. W. (1977), "Real-Time Detection and Location of Local Seismic Events in Central California," BSSA, 67, pp. 433-452.

Abstract: A computer-based system dedicated full time to automatic detection and location of local seismic events in central California has been developed. The system monitors 108 short-period vertical-component stations from the U.S. Geological Survey central California and Oroville seismic networks. Locations and magnitudes, when determined, are printed out along with first arrival times, within 2 to 5 minutes after an event occurs. Wave onsets must be clear and impulsive for best results. For this reason, regional events and teleseisms are usually rejected.

The best results have been obtained for the relatively dense, 16-station Oroville network. For the month of October 1975, 107 (91 percent) of the 118 events timed by hand were also timed and located by the real-time system. An additional eight events (7 percent) were detected in real-time but were not successfully located. Of the 107 events for which both

Stewart, S. W. (Continued)

on-line and hand-timed locations are available, 92 percent of the on-line locations are within 2 km of the epicenters determined by hand-timing.

During October 1975 the real-time system monitored 91 of the 150 stations of the central California network. Of the 260 events located by hand-timing, 225 (86 percent) were detected by the real-time system. Magnitudes of detected events range from 0.8 to 2.9. Approximately 95 percent of the events of magnitude 1½ and greater detected and located by hand-timing methods were also detected by the real-time system. Differences between hypocentral locations based on hand-timed and computer-timed arrivals may vary from 0.1 to 5 minutes of latitude or longitude.

Swindell, W. H. and N. S. Snell (1977), "Station Processor Automatic Signal Detection System. Phase 1: Final Report, Station Processor Software Development," Texas Instruments Report No. ALEX(01)-FR-77-01, AFTAC Contract No. FOR806-76-C-0025, Texas Instruments, Incorporated, Dallas, Texas.

Abstract: This report summarizes the results of a program to develop an automatic short-period signal detector for the Station Processor system. Of the two types of detectors considered, the Fisher detector and the conventional power detector, the power detector was found to be superior both in terms of signal response and false alarm statistics. A new means of setting the alarm threshold was developed. This technique produces a constant false alarm rate detector and represents a significant improvement over presently used schemes. A detection analyzer which reduces redundant detections from signal coda also was developed. A structure for the prototype detection system was designed and recommended.

Unger, R. T. (1978), "Automatic Detection, Timing and Preliminary Discrimination of Seismic Signals with the Instantaneous Amplitude, Phase and Frequency," Texas Instruments Report No. ALEX(01)-TR-77-04, AFTAC Contract No. F08606-77-C-0004, Texas Instruments, Incorporated, Dallas, Texas.

Abstract: The feasibility is evaluated of applying instantaneous amplitude, phase and frequency measurements to automatically detect, time and identify seismic events. Detection based on phase measurements is shown to be in principle 6 dB more sensitive than detection based on amplitude measurements. A phase detection and timing algorithm, using a priori known dispersion characteristics, is demonstrated to time the onset of simulated teleseismic long-period surface waves within 30 seconds accuracy in 70% of the tested cases, for waveforms down to 0 dB signal-to-noise ratio. By phase measurement, rather than by amplitude measurement, this algorithm also provides a measure of the surface wave signal-to-noise ratio. These results can be applied in the extraction of weak surface waves.

Phase detection of teleseismic short-period bodywaves was found to be unfeasible, due to the interference of early-arriving secondary signals. Therefore, short-period P-wave detection and timing are performed essentially by envelope peak detection; instantaneous frequency measurements are also used in the timing process. Tested on a small data base, this method resulted in 81% to 94% detection at 7 to 20 false alarms per hour, with signal-to-noise ratio thresholds of 2 to 3 dB. The RMS timing error, relative to analyst picks, was 0.21 seconds, comprising 84% of the test cases; this timing error apparently was independent of the signal-to-noise ratio. In some cases, however, noise can obscure the true signal onset for the analyst as well as for the automatic timing algorithm. Emergent signals may cause timing errors of several seconds. Measurements of the

Unger (Continued)

instantaneous frequency permit analysis of the delay times of secondary signals partially overlapping with earlier primary signals, down to the primary signal detection level.

Simultaneous measurements of the mean instantaneous frequency and the amount of instantaneous phase fluctuation over the first few seconds after the short-period primary signal onset provided significant separation between the populations of shallow Eurasian earthquakes, Russian presumed nuclear explosions (including peaceful explosions), and Nevada Test Site presumed nuclear explosions, even at signal-to-noise ratios below 0 dB.

Vanderkulk, W., F. Rosen and S. Lorenz (1965), "Large Aperture Seismic Array Signal Processing Study," IBM Final Report, ARPA Contract SD-296, International Business Machines, Rockville, Maryland

Abstract: This report presents the results of a five-month study, entitled "LASA Signal Processing Study" (SD-296), performed by IBM for the Advanced Research Projects Agency to:

1. Define the Large-Aperture Seismic Array (LASA) signal processing requirements.
2. Specify the characteristics of equipments required to implement the processing requirements.
3. Define an experimental program to calibrate and evaluate the signal processing equipments.

Section 1, System Description, fulfills the requirements defined under item 1. Section 2, Parametric Analysis, evaluates those parameters whose physical values determine the numerics of the LASA processing requirements and complements Section 1.

Section 3, Processing System Configuration, fulfills the requirements of item 2 by describing the overall system in terms of realizable digital hardware.

Vanderkulk (Continued)

Within Section 4, Special Problems, fulfillment of item 3, through the subsection entitled Experimental Steering Delay Determination, is obtained. In addition, other topics of interest are included to indicate specific areas of study that the work accomplished has identified. Within the mathematical appendixes are included the pertinent analytical studies performed, together with detailed program listings and numerical examples.

Section 5, Conclusion and Recommendations, outlines the next logical steps in a program designed to acquire a LASA signal processing capability.

VI. REFERENCES

- Allen, R. V., 1978, "Automatic Earthquake Recognition and Timing from Single Traces," Bull. Seism. Soc. Amer., 68, pp. 1521-1532.
- Bendat, J. S., and A. G. Piersol, 1971, "Random Data: Analysis and Measurement Procedures," Wiley Interscience, New York.
- Bracewell, R. M., 1965, "The Fourier Transform and its Applications," McGraw-Hill, New York.
- Farnbach, J. S., 1975, "The Complex Envelope in Seismic Signal Analysis," Bull. Seism. Soc. Amer., 65, pp. 951-962.
- Farrell, W. E., Wang, .., Archambeau, C. B., and Goff, R. C., 1980, "Evaluation of the MARS Seismic Event Detector," Systems, Science and Software Technical Report SSS-R-81-4656.
- Freiburger, W. F., 1963, "An Approximate Method in Signal Detection," Quarterly App. Math., 20, pp. 373-378.
- Goforth, T., and E. Herrin, 1980, "An Automatic Seismic Signal Detection Algorithm Based on the Walsh Transform," Semi-Annual Technical Report, Dallas Geophysical Laboratory, Southern Methodist University, DARPA Contract No. F49620-76-C-0030.
- LaCoss, R. T., 1972, "Variations of False Alarm Rates of NORSAR," Seismic Discrimination Semiannual Technical Summary, Lincoln Laboratory, MIT, Cambridge, MA., June, pp. 53-57.
- Helstrom, C. W., 1968, "Statistical Theory of Signal Detection," Pergamon Press.
- Masso, J. F., C. B. Archambeau, and J. M. Savino, 1979, "Implementation, Testing and Specification of a Seismic Event Detection and Discrimination System," Systems, Science and Software Report SSS-R-79-3693.
- Moltshan, G. M., V. F. Pisarenko, and N. A. Smirnova, 1964, "Some Statistical Methods of Detecting Signals in Noise," Geophys. J. R. Astr. Soc., 8, pp. 309-323.
- Sax, R. L., 1974, "Seismic Network Systems Study, Special Report No. 17, Extended Array Evaluation Program", Texas Instruments Report ALEX(01)-STR-74-01, AFTAC Contract F33657-72-C-0725, Texas Instruments Incorporated, Dallas, TX.
- Sax, R. L., J. Chen, W. W. Shen, and L. C. Weltman, 1979b, "Evaluation of Short- and Long-Period Adaptive Beamforming Processors," Technical Report No. 8, ENSCO Report No. SAR(01)-TR-79-08, ENSCO, Inc. Springfield, VA (under VSC review).

- Secoy, J. B., 1978, "Det. 459 Automatic Signal Detection (ASD) Evaluation Report," AFTAC-TR-78-54, Patrick Air Force Base, Florida.
- Shensa, M. J., 1977, "The Deflection Detector, Its Theory and Evaluation on Short-Period Seismic Data," TR-77-03, Texas Instruments, Alexandria, Virginia.
- Steinberg, J. C., and T. G. Birdsall, 1966, "Underwater Sound Propagation in the Straits of Florida, J. Acoust. Soc. Am., 39, pp. 301-315.
- Stewart, S. W., 1977, "Real-Time Detection and Location of Local Seismic Events in Central California," Bull. Seism. Soc. Amer., 67, pp. 433-452.
- Swindell, W. H., and N. S. Snell, 1977, "Station Processor Automatic Signal Detection System, Phase I: Final Report, Station Processor Software Development," Texas Instruments Report No. ALEX(01)-TR-77-01, AFTAC Contract Number F08606-76-C-0025, Texas Instruments Incorporated, Dallas, Texas.
- Unger, R., 1978, "Automatic Detection, Timing and Preliminary Discrimination of Seismic Signals with Instantaneous Amplitude, Phase and Frequency," Texas Instruments Report No. ALEX(01)-TR-77-04, AFTAC Contract Number F08606-77-C-0004, Texas Instruments Incorporated, Dallas, TX.
- Unger, R., and R. Veenkant, 1967a, "Underwater Sound Propagation in the Straits of Florida: The MIMI Experiment of 3 and 4 February, 1965," Technical Report No. 183, Cooley Electronics Laboratory, The University of Michigan, Ann Arbor, MI.
- Unger, R., and R. Veenkant, 1967b, "Underwater Sound Propagation in the Straits of Florida: The MIMI Continuous and Sampled Receptions of 11, 12, and 13 August, 1966," Technical Report No. 186, Cooley Electronics Laboratory, The University of Michigan, Ann Arbor, MI.
- Vanderkulk, W., F. Rosen, and S. Lorenz, 1965, "Large Aperture Seismic Array Signal Processing Study," IBM Final Report, ARPA Contract SD-296, International Business Machines, Rockville, Md.

APPENDIX A: BIBLIOGRAPHY OF SEISMIC EVENT DETECTORS

- Allen, R. V., 1978, "Automatic Earthquake Recognition and Timing from Single Traces," Bull. Seism. Soc. Amer., 68, pp. 1521-1532.
- Ambuter, B. P. and S. C. Solomon, 1974, "An Event-Recording System for Monitoring Small Earthquakes," Bull. Seism. Soc. Amer., 64, pp. 1181-1188.
- Anderson, K. R., 1979, "Seismic Discrimination," Semiaannual Technical Review, Lincoln Laboratory, Lexington, MA, pp. 9-11.
- Barnard, T. P., 1973, "Simulated On-Line Adaptive Processing Results Using Alaska Long Period Array Data," Special Report No. 2., Texas Instruments Incorporated, Dallas, Texas.
- Berteussen, K. A., and E. S. Husebye, 1972, "Predicted and Observed Seismic Event Detectability of the NORSAR Array," NORSAR Technical Report No. 42, NRNF/NORSAR, Kjeller, Norway.
- Black, D. G., and S. S. Lane, 1975, "An Automatic Seismic Detection Algorithm," Texas Instruments Report No. ALEX(01)-TR-75-07, Contract Number F08606-75-C-0029, Texas Instruments Incorporated, Dallas, Texas.
- Blandford, R. R., 1970, "An Automatic Event Detector at TFO," Seismic Data Laboratory Report No. 263, Teledyne Geotech.
- Blandford, R. R., 1972, "Qualitative Properties of the F-Detector, Contract Number F33657-72-C-0009, prepared for ARPA, Teledyne Geotech.
- Blandford, R. R., 1974, "An Automatic Event Detector at the Tonto Forest Seismic Observatory," Geophysics, 39, pp. 633-643.
- Blandford, R. R., 1980, "Experimental Design for Detector Evaluation: Single Channel Detectors," VSC Technical Note 38.
- Blandford, R. R., and D. M. Clark, 1971, "Seismic Array Design," Report No. SDL-267, Seismic Data Laboratories, Teledyne Geotech, Alexandria, Virginia.
- Blandford, R. R., and M. W. Wirth, 1973, "Automatic Array and Network Detection in the Presence of Signal Variability," Report No. SDL-308, Seismic Data Laboratories, Teledyne Geotech, Alexandria, Virginia.
- Booker, A. H., 1965, "Analysis of Variance as a Method for Seismic Signal Detection," Seismic Data Laboratory Report No. 116, Teledyne Earth Sciences.

- Bungum, H. and E. S. Husebye, 1973, "Analysis of the Operational Capabilities for Detection and Location of Seismic Events at NORSAK," Bull. Seism. Soc. Amer., 64, pp. 637-656.
- Capon, J., 1961, "On the Asymptotic Efficiency of Locally Optimum Detectors," IRE Trans. Inf. Theory 7, pp. 67-71.
- Capon, J., R. J. Greenfield, R. J. Kolker, and K. T. Lacoss, 1968, "Short-Period Processing Results for the Large Aperture Seismic Array," Geophysics, 33, pp. 452-472.
- Chang, A. C., R. M. Seggelke, and R. R. Baumstark, 1976, "The Effect of Band Pass Filters on LASA Detection Performance," SDAC-TR-75-9, Teledyne Geotech, Alexandria, Virginia.
- Claerbout, J. F., 1964, "Detection of P-waves from Weak Sources at great distances," Geophysics, 29, pp. 127-211.
- Cochran, M. D., 1973, "Seismic Signal Detection Using Sign Bits," Geophysics, 39, No. 6, pp. 794-810.
- Dash, B. P., B. L. A. Hains, 1974, "Moveout Detection by an Auto-correlation Matrix Method," Geophysics, 39, No. 6, pp. 794-810.
- De Braemacker, J. C., 1964, "Detection of Small Arrivals," Bull. Seism. Soc. Amer., 54, pp. 2141-2164.
- Dean, W. C., 1975, "Operational Experience with the LSAS/SAAC System," In Exploitation of Seismograph Networks, NATO Advanced Study Institute, Series E., 11, pp. 149-164.
- Eterno, J. S., D. S. Burns, L. J. Freier, and S. W. Buck, 1974, "Special Event Detection for an Unattended Seismic Observatory", Report R-765, ARPA Contract F44620-73-C-0057, Charles Stark Draper Laboratory, Inc, Cambridge, Mass.
- Farnbach, J. S., 1975, "The Complex Envelope in Seismic Signal Analysis," Bull. Seism. Soc. Amer., 65, pp. 951-962.
- Farrell, W. E., Wang, J., Archambeau, C. B., and Goff, R. C., 1980, "Evaluation of the MARS Seismic Event Detector," Systems, Science and Software Technical Report SSG-R-81-4656.
- Frasier, C. C., 1973, "Seismic Discrimination," Semiannual Technical Review, Lincoln Laboratory, Lexington, MA, pp. 75-76.
- Freiberger, W. I., 1963, "An Approximate Method in Signal Detection," Quarterly App. Math., 20, pp. 373-378.
- Gendzwill, D. J., Z. Hajnal, and J. Arnold, 1979, "A Computer Controlled Seismic System with a Novel Pattern Recognition Program," Abstract, EOS, 60, No. 42, p. 755.

- Gjoystdal, H., and E. S. Husebye, 1972, "A Comparison of Performance Between Prediction Error and Bandpass Filters," NORSAR Technical Report 48, Royal Norwegian Council for Scientific and Industrial Research, Kjeller, Norway.
- Goforth, T. T., and Herrin, E., 1980, "An Automatic Seismic Signal Detection Algorithm Based on the Walsh Transform", Semi-Annual Technical Report, Dallas Geophysical Laboratory, Southern Methodist University, DARPA Contract No. F49620-76-C-0030.
- Green, P. W., E. J. Kelley, and M. J. Levin, 1966, "A Comparison of Seismic Array Processing Methods," Geophysics Journal, 11, pp. 67-84.
- Helstrom, C. W., 1968, "Statistical Theory of Signal Detection, Pergamon Press.
- Husebye, E. S., 1972, "NORSAR Research and Development (1 July 1971, 30 June 1972)," NORSAR Report No. 50, Royal Norwegian Council for Scientific and Industrial Research, Kjeller, Norway.
- Kennett, B. L. N. 1974, "Short-term Spectral Analysis and Sequency Filtering of Seismic Data." NATO Advanced Study Institute, Sanderfjord, "Exploitation of Seismograph Networks," (Ed. K. G. Beauchamp), Noordhoff Int. Publ. Co., Leiden, Netherlands.
- Lacoss, R. T., 1972, "Variations of False Alarm Rates of NORSAR," Seismic Discrimination Semiannual Technical Summary, Lincoln Laboratory, Massachusetts Institute of Technology, Cambridge, Massachusetts, June 1972, pp. 53-57.
- Lane, S. S., 1974, "Preliminary Comparison of Automatic Fisher and Conventional Power Detection Algorithms," Texas Instruments Report No. ALEX(01)-STR-73-16, Contract Number F33657-72-C-0725, Texas Instruments Incorporated, Dallas, Texas.
- Lane, S. S., 1974, "Study of Two Automatic Short-Period Signal Detectors," Texas Instruments Report No. ALEX(01)-TR-74-09, Contract Number F08606-74-C-0033, Texas Instruments Incorporated, Dallas, Texas.
- Lintz, Paul R., 1976, "Array Design and Algorithms for Omnidirectional Detection and Estimation of Seismic Events," PH.D. dissertation, the Catholic University of America, Washington, D.C.
- Masso, J. F., C. B. Archambeau, and J. M. Savino, 1979, "Implementation, Testing and Specification of a Seismic Event Detection and Discrimination System," Systems, Science and Software Report SSS-R-79-3963.

- McCowan, D. W., 1975, "Seismic Discrimination," Semiannual Technical Review, Lincoln Laboratory, Lexington, MA pp. 28-29.
- Melton, B. S., and Bailey, L. F., 1957, "Multiple Signal Correlators," Geophysics, 22, pp. 565-588.
- Melton, B. S., and Karr, L. F., 1957, "Polarity Coincidence Scheme for Revealing Signal Coherence," Geophysics, 22, pp. 553-564.
- Moltshan, G. M., V. F. Pisarenko, and N. A. Smirnova, 1964, "Some Statistical Methods of Detecting Signals In Noise," Geophys. J. R. Astr. Soc., 8, pp. 309-323.
- Muirhead, K. J., 1968, "Eliminating False Alarms When Detecting Seismic Events Automatically," Nature, 217, pp. 533-534.
- Muirhead, K. J., and R. Datt, 1976, "The N-th Root Process Applied to Seismic Array Data," Geophysics, J. R. Astr. Soc., 47, pp. 197-210.
- Ringdal, F. E., E. S. Hysebye, and A. Dahle, 1972, "Event Detection Problems Using a Partially Coherent Seismic Array," NORSTAR Technical Report 45, Royal Norwegian Council for Scientific and Industrial Research, Kjeller, Norway.
- Savino, J. M., J. F. Masso, and C. B. Archambeau, 1979, "Discrimination Results from Priority 1 Stations," Systems, Science and Software, Report SSS-CR-79-4026, San Diego, California.
- Sax, R. L., 1974, "Seismic Network Systems Study, Special Report No. 17, Extended Array Evaluation Program, Texas Instruments Report ALEX (01)-STR-74-01, AFTAC Contract F33657-72-C-0725, Texas Instruments Incorporated, Dallas, TX.
- Sax, R. L., 1976, "Design, Simulated Operation, and Evaluation of a Short-Period Seismic Discrimination Processor in the Context of a World-Wide Seismic Surveillance System," Technical Report No. 9, Texas Instruments Report No. ALEX(01)-TR-76-09, Texas Instruments, Incorporated, Dallas, Texas.
- Sax, R. L., 1980, "Review of the Seismic Detectors Developed and/or Evaluated by Texas Instruments (TI) at ENSCO", Report SAR (01)-TM-80-01, ENSCO Inc., Alexandria, Va.
- Sax, R. L., A. G. R. Beil, and D. L. Dietz, 1979a, "Event Identification Experiment: Priority II Data Set, Technical Report No. 6, ENSCO Report No. SAR(01)-TR-79-06, ENSCO, Inc., Springfield, VA (under VSC review).

- Sax, R. L., J. Chen, W. W. Shen, and L. C. Weltman, 1979b, "Evaluation of Short- and Long-Period Adaptive Beamforming Processors," Technical Report No. 8, ENSCO Report No. SAR(01)-TR-79-08, ENSCO, Inc. Springfield, VA (under VSC review).
- Secoy, J. B., 1978, "Det. 459 Automatic Signal Detection (ASD) Evaluation Report," AFTAC-TR-78-54, Patrick Air Force Base, Florida.
- Shen, W. W., 1974, "Comparison of Coherent and Incoherent Beamforming Envelope Detectors for NORSAR Regional Seismic Events," Technical Report No. 6, Texas Instruments Report No. ALEX(01)-TR-74-06, AFTAC Contract Number F08606-74-C-0033, Texas Instruments Incorporated, Dallas, Texas.
- Shen, W. W., 1979, "A Constrained Minimum Power Adaptive Beamformer with Time-Varying Adaptation Rate," Geophysics, 44, No. 6., pp. 1088-1096.
- Shensa, M. J., 1977, "The Deflection Detector, Its Theory and Evaluation on Short-Period Seismic Data," TR-77-03, Texas Instruments, Alexandria, Virginia.
- Shoup, E. M., and R. L. Sax, 1974, Simulation of a World-Wide Seismic Surveillance Network," Texas Instruments, Report No. ALEX(01)-TR-74-13, Contract Number F08606-74-C-0033, Texas Instruments Incorporated, Dallas, Texas.
- Shumway, R. H., 1971, "On Detecting a Signal in N Stationarily Correlated Noise Series," Technometrics, 13, pp. 499-519.
- Steinberg, J. C., and T. G. Birdsall, 1966, "Underwater Sound Propagation in the Straits of Florida, J. Acoust. Soc. Am., 39, 301-315.
- Stewart, S. W., 1977, "Real-Time Detection and Location of Local Seismic Events in Central California," Bull. Seism. Soc. Amer., 67, pp. 433-452.
- Swindell, W. H., and N. S. Snell, 1977, "Station Processor Automatic Signal Detection System, Phase I: Final Report, Station Processor Software Development", Texas Instruments Report No. ALEX(01)- FR-77-01, AFTAC Contract Number F08606-76-C-0025, Texas Instruments Incorporated, Dallas, Texas.
- Unger, R., 1974, "Estimating a Seismic Station's Detection Capability from Noise, Application to VLPE Stations," Texas Instruments, Report No. TI-ALEX(01)-TR-74-04.
- Unger, R., 1976a, "Seismic Event Discrimination Using the Instantaneous Envelope, Phase and Frequency," Abstract, EOS, 57, p. 286.

- Unger, R., 1976b, "A Time-Variant Wiener Filter for Dispersed Waveforms," Texas Instruments Report No. ALEX(01)-TR-76-08, AFTAC Contract Number F08606-76-C-0011, Texas Instruments Incorporated, Dallas, Texas.
- Unger, R., 1976c, "The Instantaneous Phase of Long-Period Waveforms," Abstract, EOS, 57, p. 759.
- Unger, R., 1978, "Automatic Detection, Timing and Preliminary Discrimination of Seismic Signals with Instantaneous Amplitude, Phase and Frequency," Texas Instruments Report No. ALEX(01)-TR-77-04, AFTAC Contract Number F08606-77-C-0004, Texas Instruments Incorporated, Dallas, TX.
- Unger, R., 1978, "Short-Period Noise Envelope Statistics: A Basis for Envelope Detector Design," Texas Instruments Report No. ALEX(01)-TR-78-05, Texas Instruments Incorporated, Dallas, TX.
- Ursin, B., 1979, "Seismic Signal Detection and Parameter Estimation," Geophysical Prospecting, 27, pp. 1-15.
- Vanderkulk, W., F. Rosen, and S. Lorenz, 1965, "Large Aperture Seismic Array Signal Processing Study," IBM Final Report, ARPA Contract SD-296, International Business Machines, Rockville, Md.
- Veith, K. F., 1977, "A Digital Event Detector," Abstract, EOS, 58, p. 1190.
- Veith, K. F., 1978, "Seismic Signal Detection Algorithm," Technical Note 1/78, Teledyne Geotech, Garland, TX.
- Von Seggern, D. H., and R. R. Blandford, 1966, "Observed Variation in the Spectral Ratio Discriminant From Short-Period P Waves," Technical Report No. SDAC-TR-76-12, Seismic Data Analysis Center, Teledyne Geotech, Alexandria, Virginia.
- Von Seggern, D., and R. R. Blandford, 1976, "Seismic Threshold Determination," Bull. Seism. Soc. Amer., 66, pp. 753-788.
- Weichert, D. H., 1975, "Reduced False Alarm Rates in Seismic Detection Using Non-Linear Beamforming," Geophysics Research Letters, 2, pp. 121-123.
- Weichert, D. H., and M. Henger, 1976, "The Canadian Seismic Array Monitor Processing System (CANSAM)," Bull. Seism. Soc. Amer., 66, No. 4. pp. 1331-1403.
- Wirth, M. H., R. R. Blandford, and R. H. Shumway, 1971, "Automatic Network Detection," Seismic Data Laboratory Report No. 285, Teledyne Geotech.

Wirth, M. H., R. R. Blandford, and R. H. Shumway, 1976, "Automatic Seismic Array and Network Detection," Bull. Seism. Soc. Amer., 66, pp. 1375-1380.

Yuen, C. K., 1973, "A Fast Algorithm for Computing Walsh Power Spectrum," in 1973 Proceedings; Applications of Walsh Functions, Washington, D.C.